University of Nevada Reno

Susceptibility of Headwater Catchment Hydrology to Persistent Droughts and Forest Structure Modification – A Plot to Catchment Scale Analysis

A thesis submitted in partial fulfillment of the
requirements for the degree of Masters of Science in
Hydrogeology

By

Rowan Gaffney

Dr. Scott Tyler/ Thesis Advisor

December, 2016

THE GRADUATE SCHOOL

We recommend that the thesis
prepared under our supervision by

ROWAN GAFFNEY

Entitled

Susceptibility Of Headwater Catchment Hydrology To Persistent Droughts And Forest Structure Modification – A Plot To Catchment Scale Analysis

be accepted in partial fulfillment of the
requirements for the degree of

MASTER OF SCIENCE

Dr. Scott Tyler, Advisor

Dr. Gordon Grant, Committee Member

Dr. Adrian Harpold, Graduate School Representative

David W. Zeh, Ph.D., Dean, Graduate School

December, 2016

Abstract

Headwater catchments across the Western United States are critical environments to natural ecosystems and are a vital component of water resources to many communities and industries and may be strongly affected by changing climate and altered disturbance regimes. To better quantify how these systems may be affected by climate change and to develop more precise management strategies to mitigate the negative impacts, two studies were conducted at a plot scale in Lassen National Forest and at a regional scale across the Sierra Nevada's. The first chapter addresses how forest management strategies such as thinning alter the soil moisture and sap flow dynamics during a severe drought. The reduced forest density across the thinned forest prolonged the initiation of the soil moisture recession, resulting in more available water later in the growing season. Furthermore, across the study area, a threshold response of sap flow velocity to low soil moisture levels was observed. The second chapter asserts a novel methodology to quantify the storage-flow relationship in headwater catchments across the Sierra Nevada's using space based estimates of storage. A framework is then developed based on the storage-flow relationship and catchment hydrogeology to inform catchment susceptibility to decreasing flows at increasing drought severity. The results suggest that, at increasing drought severity, high storage capacity catchment flows are reduced at a greater rate than low storage capacity catchments.

Table of Contents

List of Tables

List of Figures

Headwater catchments across the Western United States are critical environments to natural ecosystems and are a vital component of water resources to many communities and industries and may be strongly affected by changing climate and altered disturbance regimes. Ecological perturbations in the form of management, such as fuel-reduction treatments, and natural disturbances, such as wildland fire and bark beetle infestations, are common in many headwater catchments and may strongly affect the hydrologic system through changes in forest structure. Yet, currently there lacks a robust understanding of how modifications to forest structure may affect the hydrologic system. These disturbances are predicted to become more severe with climate change in the western US (Allen et al., 2010; Westerling et al., 2006; Williams et al., 2012), highlighting the importance of understanding how forest structure alters the hydrologic system.

For mountainous headwater catchments, the most critical hydrologic components that are impacted by forest structure modifications are soil moisture dynamics, snowpack accumulating and ablation, and net evapotranspiration. Chapter 1 of this proposal attempts to resolve some of these questions at the plot-scale in a managed and heavily instrumented study area in Lassen National Forest. However, the confluence of active forest management and changing climate regimes make deciphering the long-term hydrologic impact of both these disturbances challenging.

Changing climate regimes have the potential to greatly alter the eco-hydrologic dynamic of headwater catchments, independent of changes in forest structure. The probable increase in frequency and severity of droughts associated with climate change, as seen in the ongoing 2012 drought, has the potential to reduce water resources and stress ecological communities. Chapter 2 of this proposal will put forward a framework to inform catchment susceptibility to

decreasing flows due to increasing drought severity. This framework will be based on a novel approach to quantify the storage-flow dynamic of each catchment and how it relates to catchment hydrogeology. Together, these two chapters will provide important insights into how forest disturbance regimes and climate change will affect catchment hydrology by resolving plot-scale mechanisms (Chapter 1) and a regional analysis to understand broad patterns (Chapter 2). Climate change alters the fundamental energy balance and mass conservations within these systems. Therefore, it is expected that the historical dynamics within these systems will be altered. Comparing the results of these two studies from disparately different scales will illustrate the impact changing climatic conditions can have across scales due to altering the timing and environmental gradients within the hydrologic system. Better understanding how these systems will be fundamentally transformed is critical to developing management strategies that will improve ecological and hydrologic resources for the future.

Chapter 1: Soil Moisture and Sap Flow dynamics to Drought and Forest Management Strategies: A Case Study in Lassen National Forests

Introduction

Across the western United States increasing forest vulnerability to wildland fires, degraded ecosystem health, and stress to water resources are linked to changing climate regimes and historical firefighting practices. In response, fuel-reduction treatments are commonly employed throughout the western United States to improve forest health, increase water resources, and decrease the risk of wildland fires (“NFP (National Fire Plan),” 2010). Whereas it is clear that fuel-reduction treatments are effective at reducing fuel-loads and thus the probability of high severity wildland fires under certain climate conditions, it is unclear how these fuel-reduction treatments alter forest hydrology and water resources.

There lacks a consensus within the scientific and management community concerning the impact of forest modifications to forest/catchment hydrology. The dispute stems from the complexities and the physiographic, temporal, and spatial heterogeneity that make measuring each component within the forest hydrology system challenging. For instance, Grant and Jones (1996) found that while forest harvests and roads increased peak stream flow, this was primarily due to flow routing rather than changes in the water budget components such as evapotranspiration. To a first order, the two most critical hydrologic processes that are altered by forest modifications such as thinning are actual evapotranspiration (AET) and the snow accumulation and ablation processes. A thinned forest will likely have an initial reduction of potential evapotranspiration (AET) due to a reduction in leaf area, which may lead to an increase in recharge. However, for forests that reach a water limited state mid-summer, the thinned forests may continue to transpire later into the summer and depleting the water resources to pre-thinning levels. Therefore, the decrease in AET does not correspond to an annual net decrease in Actual Evapotranspiration (AET) and likely a minimal net increase in recharge. In such a case, the net effect of thinning may have a negligible impact on water resources but may improve forest health/vitality. Moreover, the high rate of grow-back and understory establishment may quickly reduce the initial decrease in AET and thereby result in a relatively short window of increased forest health vitality and water resources gains. Further complicating the system is the diverse range of soil characteristics that may either dampen or exacerbate the effects of thinning on AET (Garcia and Tague, 2015).

A good metric that integrates many of the eco-hydrologic processes of forested landscapes is soil moisture. Similar to stream flow at the base of catchments in watershed hydrology, soil moisture integrates many of the “upstream processes” at the plot scale within

the forest (Vereecken et al., 2008). Soil moisture dynamics are directly related to subsurface recharge (ie: gravity drainage), forest and understory transpiration, bare soil evaporation, liquid precipitation, snowmelt rates, and interception.

Soils provide a critical reserve of late-season moisture, especially in Mediterranean climates, and are pivotal to forest and ecosystem health. For Sierra Nevada forests, soils act as a secondary water reservoir following the melting of the snow pack. At the study area, soil moisture is recharged during winter and spring and is depleted through the summer and fall. Late season soil moisture is an important factor for wildland forest fire resilience and is largely dependent on the snow pack duration and soil properties. Yet, due to the complex interactions between forest biotic processes and forest hydrology, it is unclear how forest management practices impact the timing and magnitude of soil moisture dynamics.

To develop a better deterministic understanding of how the soil moisture dynamics are effected by fuel reduction treatments in mid-latitude, mediterranean forests, a set of innovative environmental monitoring and measuring techniques are being deployed in Lassen National Forest. The overall objectives of this study is to monitor the water dynamics under a variety of forest management practices. As part of this work, soil moisture and tree water uptake data will be used to evaluate and assess if the fuel reductions treatments have any measurable impact on the dynamics of the annual soil moisture dry-out or temporal trends associated with understory grow-back. It was expected to find decreased summer/fall soil moisture recession rates in forests that have undergone fuel reduction treatments. This reduction in the recession rates will largely be due to the reduced rate at which the forest can transpire. Furthermore, it was predicted that trees reach water limited states later in the year at the sites that have undergone

fuel reduction treatments. Seed trees in clear cut areas will not reach water limited states in the summer/fall as they will not be competing for deep soil moisture with neighboring trees.

Study Area

To evaluate the relationship between forest structure and plot scale hydrologic processes, a study area in the Hat Creek Basin of Lassen National Forest (Panner Unit 321, 40.6^{o} N, 121.5^{o} W, 1730 meters above sea level that consists of four sites was heavily instrumented (see Figure 1). Of the four sites, two are located in regions that had a Diversity Thinning treatment (Div-East and Div-West), one site is in a small (~2 acre) Group Selection (GS), and the fourth site is in the unmodified forest (Control). The diversity thinning management strategy involves structural thinning of the general matrix and radial release of large diameter overstory trees with ~15% of the treated area earmarked as retention islands. The overall goal of this management strategy is to promote structural diversity as well as protect and encourage the development of large overstory trees. The Group Select management strategy is designed to create an uneven-aged method of tree regeneration in small areas up to 2 acres. Within this 2 acre area all but the large seed trees will be removed. The remaining seed trees are typically greater than 30 inch DBH (diameter at breast height) and have a density of roughly 2 per acre (Kathleen S. Morse, 2008).

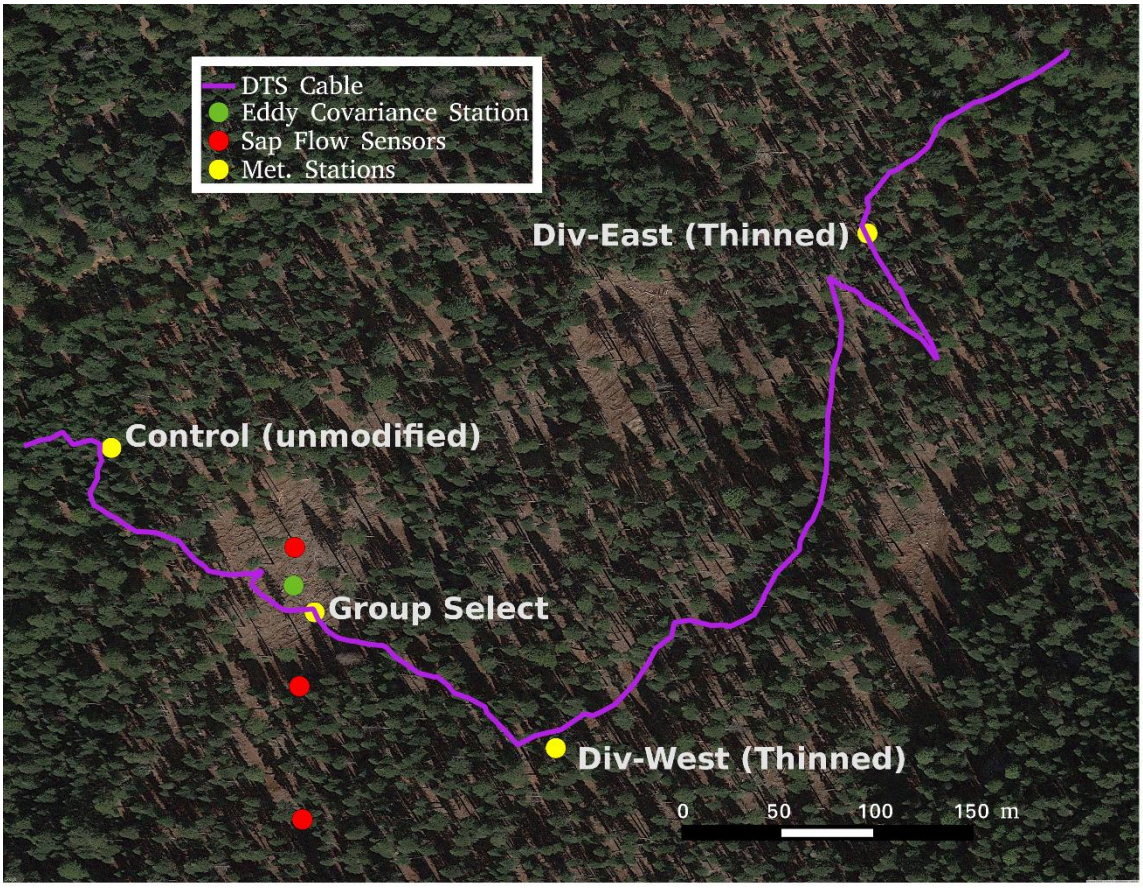

Figure 1: Overview map of study area showing the four site locations, sap flow sensors, DTS cable, and eddy covariance station.

Each site consists of an eKo PRO Series ES2000 meteorological station that measures wind speed and direction, relative humidity, barometric pressure, incoming solar radiation, and air temperature. The relative humidity, barometric pressure, incoming solar radiation, and air temperature measurements have resolutions of 1%, 0.1 mbar,1 W/m^2, and 0.1 ^{o}C, ranges of 0-100%, 880-1080 mbar, 0-1800 W/m^2, and-40-60 ^{o}C, and accuracies of 3%, 1.0 mbar, 5% and 0.5^{o}C, respectively (Memsic Inc., n.d.). Four eS1110 Decagon EC-5 soil water content sensors were instrumented at each site at 15, 30, 50, and 100 cm bgs. The soil moisture sensors use a frequency domain methodology to measure the in-situ dielectric constant which can then be

converted to volumetric soil moisture. The sensors have a stated accuracy of 2% with a resolution of .25 % (Decagon Devices, Inc., 2016). In addition to the soil moisture sensors, two soil temperature sensors at 50 and 100 cm bgs are co-located with each meteorological station. Snow poles paired with automated cameras capture the daily snow depth evolution at each site during the winter. In addition to the site level instrumentation, a 1 km Distributed Temperature System (DTS) fiber optic cable was strung through the four sites. The DTS measures temperature along the fiber optic cable at a resolution of 1 meter. During the late-winter and early spring of 2015, an eddy covariance flux tower was setup at the GS site to measure sublimation. Four trees were instrumented with paired sap flow sensors on the East and North aspects. At this time, two of the sap flow sensors (both located on the same tree) were nonoperational.

A complicating factor in comparing measurements of soil moisture across the study area is the potential spatial heterogeneity of unsaturated soil water characteristics. Soil water characteristics are predominately a function of the soil grain size distributions. Therefore, to address this issue, soil samples at each site were collected at the equivalent soil moisture measurement depths of 15, 30 ,50, and 100 cm bgs. Laser Particle Size Analysis (Malvern Mastersizer 3000) measured the soil particle distribution from .01 to 1000 micrometers. Figure 2 and 3 show the cumulative soil particle size distribution for each sample and the depth averaged deep soil as specified in Equation 1. Using the National Resources Conservation Service (NCRS) classification scheme, soils across the study area had a narrow classification range of silty loam to sandy loam. Due to the relatively homogenous soil particle size distribution across the study area, it can be inferred that the unsaturated soil water properties across the study area are relatively uniform. Therefore, it is permissible to compare the absolute magnitude of volumetric

soil moisture measurements between the study sites. Furthermore, the general coarse nature of the soils suggests that they are highly permeable.

Equation 1: $PP_{deep} = .17*PP_{30}(d) + .34*PP_{50}(d) + .49*PP_{100}(d)$

PP_{deep} = Cumulative Percent Passing for Deep Soils

$PP_{30}(d)$ = Cumulative Percent Passing at 30 cm bgs

$PP_{50}(d)$ = Cumulative Percent Passing at 50 cm bgs

$PP_{100}(d)$ = Cumulative Percent Passing at 100 cm bgs

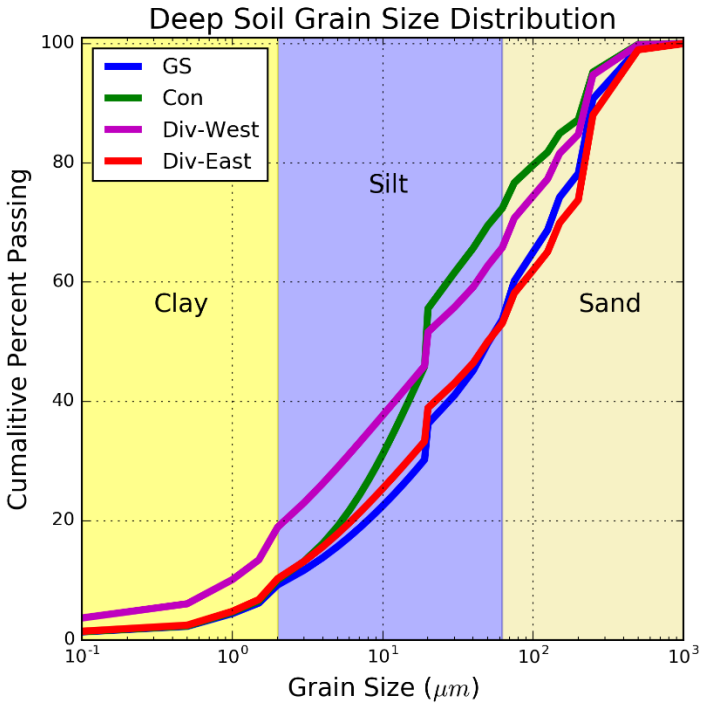

Figure 2: Grain size distribution of deep soils at the four study sites.

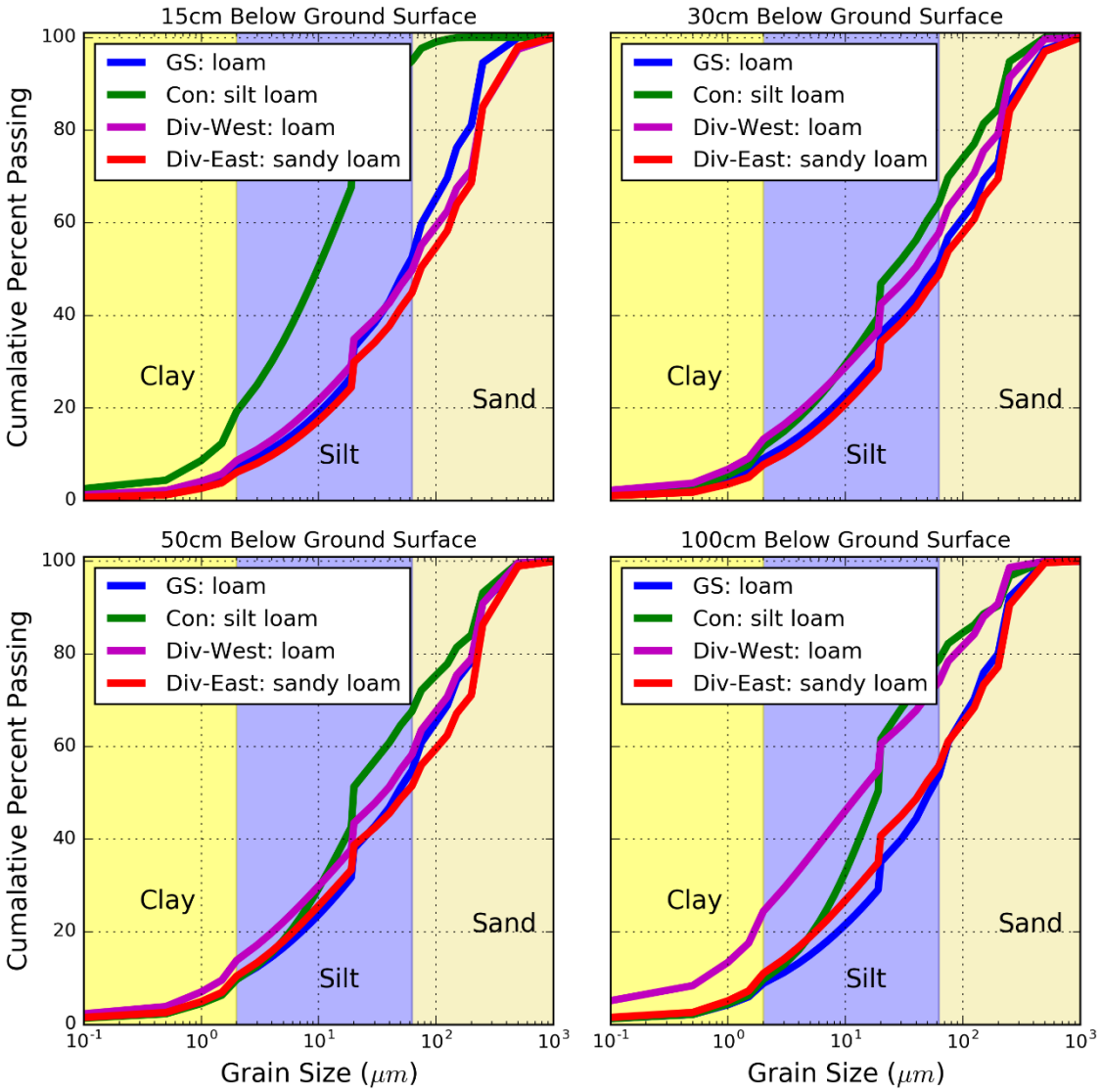

Figure 3: Grain size distributions at each soil moisture sensor depth at each study site. The National Resources Conservation Service (NCRS) classification for each soil is defined in the legend of each graph.

Sap flow sensors were instrumented to four Ponderosa Pine trees across the study area, three of which are operational, a seed tree within the Group Selection (Tree 1), a tree at the Group Selection – thinned boundary (Tree 2 – edge tree), and a tree in the thinned forest near the Div-West site (Tree 4, Figure 1). The sensors were custom built by Tranzflow NZ LTD and use

the heat pulse technique is measure sap flow velocity at 6 depths within the tree (Green et al., 2003). Each sensor consists of a heating unit and two thermistor beads located 20 mm upstream and 5 mm downstream of the heating unit. The heating unit produces a 1 second heat pulse every 30 minutes. The resulting time delay for the two thermistors to reach equal temperatures is used to calculate the sap flow velocity (Green, 1998). The selected trees had no visual evidence of damage to the stem or crown and overall appeared healthy. At each tree, two sap flow sensors are instrumented on the north and east facing aspects. Following installation, the tree was wrapped with reflective insulation. During instrumentation, many of the individual thermistor sensors were damaged or did not operate properly. For instance, the Tree 3 sensors in the thinned site never functioned properly all but one system had all 12 thermistors working. Therefore, calculating the absolute volumetric sap flux within each tree was problematic.

Methods: Soil Moisture Dynamics

The depletion/recession of soil moisture through the growing season is predominately driven by three processes: gravity drainage resulting in recharge, bare soil evaporation, and transpiration. Due to the surficial litter layer and relative course soil texture and high permeability across the study area (see above and Figure 2 and 3), bare soil evaporation will comprise a relatively small component of the mass flux within the soil and will therefore have limited impact of deep soil moisture recession (>20 cm bgs). For a typical year, snow accumulation and sublimation dynamics would strongly impact the recession dynamics, however there was no persistent snow during the 2015 winter. Due to the spatially uniformity of the soil texture/permeability measured at the site (Figure 3), gravity drainage will be a function of soil moisture content. Therefore, differences in the magnitude of soil moisture recession

dynamics between the sites during the growing season will be primarily due to understory and canopy transpiration dynamics.

Deep soil moisture was measured with eS1110 Decagon EC-5 water content sensors at 30, 50, and 100 cm bgs. To compute a deep soil moisture metric, the three measurements were integrated with a depth average approach from 22.5 to 125 cm bgs depths. Depth intervals were set as equal distances between each sensor. The 30 cm bgs soil moisture measurement was applied to the 22.5 to 40 cm bgs depth range, the 50 cm measurement was applied to the 40 to 75 cm bgs depth range, and the 100 cm measurement was applied to the 75 to 125 cm range (Equation 2).

Equation 2: $SM_{Deep} = .49*SM_{100} + .37*SM_{50} + .17*SM_{30}$
SM_{Deep} = Deep Soil Moisture
SM_{100} = Soil Moisture at 100 cm bgs
SM_{50} = Soil Moisture at 50 cm bgs
SM_{30} = Soil Moisture at 30 cm bgs

Deep soil moisture recession at the three sites was estimated by kinematic Equation 3, also referred to as a reservoir model. In the linear case (c_2=1), the decay of soil moisture takes the form of Equation 4. In the non-linear case (c_2<>1), the decay takes the form of Equation 5. An asymptote (SM_{crit}) was included in the equations due to the effect of the residual soil moisture. A lognormal decay functions was also evaluated as a potential model of the soil moisture recession (Equation 6) at the sites.

Equation 3: $S_o = c_1*SM^{c2}$
S_o = Flux of moisture out of the soil
SM = Soil Moisture (% Volume)
c_1 and c_2 = Fitting Parameters

Equation 4: $SM(t) = (SM_{init} – Sm_{crit}) * \exp(-c_1*t) + SM_{crit}$
SM(t) = Soil moisture time series

SM_{init} = Initial Soil Moisture
Sm_{crit} = Critical Soil Moisture
t = time

Equation 5: $SM(t) = (SM_{init} - SM_{crit}) * (1 - c_1*t)^{c2/(c2-1)} + SM_{crit}$
SM(t) = Soil moisture time series
SM_{init} = Initial Soil Moisture
Sm_{crit} = Critical Soil Moisture
t = time

Equation 6: $SM(t) = SM_{init} + (-c_3*LN(t))$
SM(t) = Soil moisture time series
SM_{init} = Initial Soil Moisture
C_3 = Fitting Parameter
t = time

The initiation of the soil moisture recession during the 2015 growing season was variable across the study sites. An empirical approach was implemented to calculate the timing of the initiation at each site. The date of the onset of the recession was calculated as the latest date the soil moisture was at a cut-off of 5% below the January 1st to May 1st mean value. In a typical year at the study area, the start of the soil moisture recession would be directly correlated to the snow disappearance date. However, due to the uncharacteristically warm winter, little to no snow accumulated at the site. Therefore, the initiation of the recession will be more closely related to precipitation and interception dynamics at each site. The characteristic time scale for each recession was calculated as the point when ~63 percent ($1/e^1$) of the recession had completed.

Methods: Soil Moisture and Sap Flow Dynamics

Sap Flow sensors measure sap uptake velocity at several trees across the study site. Due to instrumentation challenges (see above), estimating the volumetric sap flux was deemed less desirable than using the sap velocity measurement. Sap flow velocity was considered a sufficient

measurement because the primary objective was to quantify how environmental variables, such as soil moisture, humidity, wind speed and solar radiation, limit transpiration. Therefore, the time series of average sap velocity at each tree, rather than the absolute volumetric flux, is sufficient to characterize the sap flow and transpiration dynamics. For each tree, all the operating sensor were averaged at one hour intervals to result in a single sap velocity in units of centimeters per hour. For much of the analysis, rather than using the absolute value of the measurements, the relative changes and trends in each time series was used to quantify the transpiration dynamics.

Limitations to transpiration/sap flow for healthy trees during the growing season are primarily a function of available water and PET. Other secondary factors such as light and temperature dynamics are considered negligible components within the framework of this study. PET is driven by net radiation and the vapor pressure gradient. Therefore, sap flow velocities were analyzed across the three instrumented trees as a function of deep soil moisture, incoming solar radiation, relative humidity, and wind speed derived from the micro-metrological measurements. The combinations of these four measurements should capture the water availability, net radiation, and vapor pressure gradient dynamics at each site. Critical to understanding how forest management and fuel reduction treatments impact forest hydrology is determining the timing and magnitude of forests transitioning from an energy limited to a water limited state. De-convolving the impact of the dependent variables on the sap velocity is challenging due to the competing, and often opposing and correlated nature of soil moisture, solar radiation, and relative humidity. To decompose this process and better quantify the individual influence of solar radiation, soil moisture, wind speed, and relative humidity on sap flow, a multiple regression linear model was implemented to the mean day time data at each

site/tree. The linear model will show the magnitude and significance that each of the explanatory variables will have on sap flow. Ultimately, this analysis will define the degree of water or energy limitation to transpiration for the instrumented trees.

The historically anomalous drought conditions across California during the summer of 2015 provided a unique opportunity to test for a threshold response of sap flow to low soil moisture levels. The nearby NWS (National Weather Service) Coop Station at Manzanita Lake measured 79% (~83 centimeters, Figure 4) of historical precipitation for the 2015 water year. While the 2015 reduction in precipitation does not appear to be extreme, it does not account for the cumulative effects of reduced precipitation from previous years or the increased temperatures. A more complete view of the drought is provided by the United States Drought Monitor. For the Lower Pit River watershed (8 digit HUC: 18020003) where the study area is located, nearly the entire region was in a state of extreme drought and half the watershed was classified as in a state of exceptional drought, the most extreme category (Figure 5). The cumulative effect of the drought is also evident in the average annual (water year) precipitation presented in Figure 4. For instance, since 1955, the historic 4 year (water year) average minimum occurred during 2015 water year.

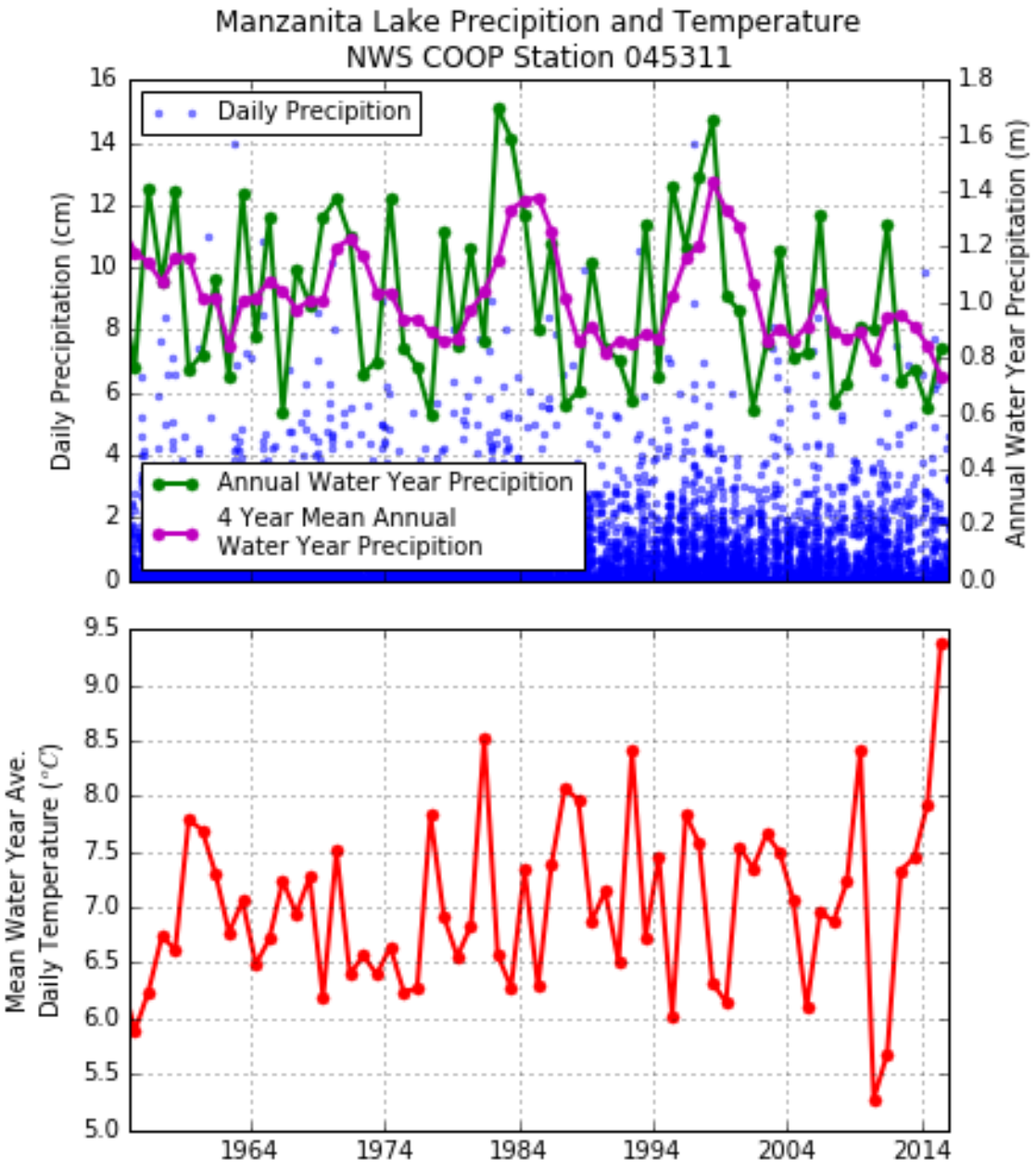

Figure 4: Precipitation and average daily temperature data from NWS COOP station 045311 at Manzanita Lake. Daily precipitation, annual (water year) precipitation and temperature, and a 4 year average annual (water year) time series are shown.

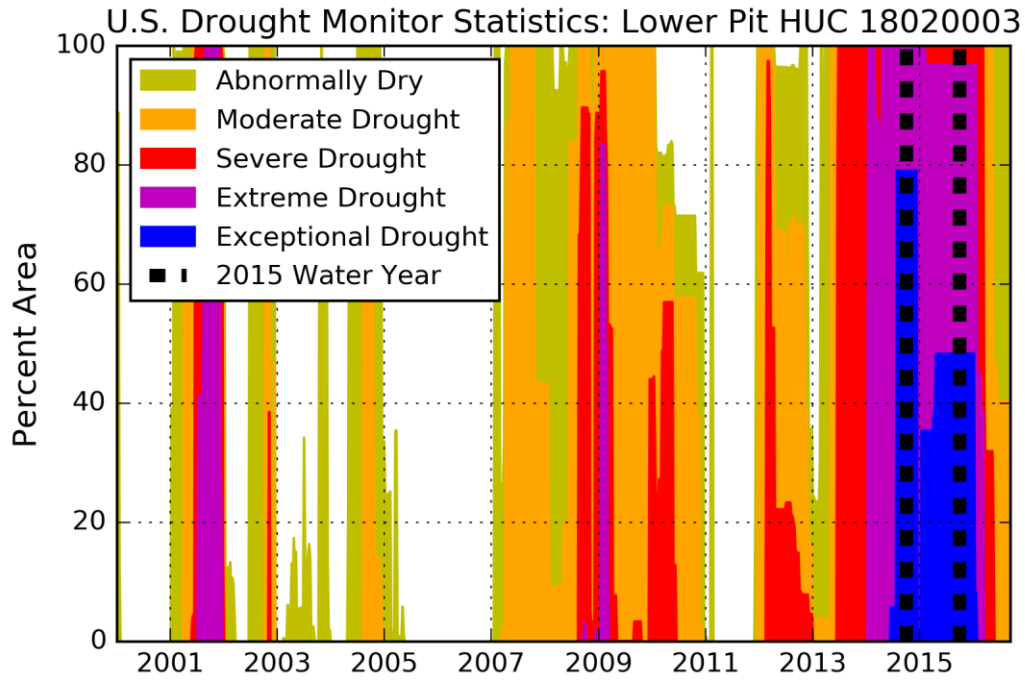

Figure 5: Time series of drought severity and percent area from the United States Drought Monitor for the Lower Pit HUC (18020003). The 2015 water year is bracketed with thick dashed vertical lines.

Due to the drought, soils will likely be at uncharacteristically low soil moisture levels. At low soil moisture levels, trees may lose the ability to extract water due large capillary forces / suction soils will exhibit on the water molecules. Therefore, the data was analyzed for a low soil moisture threshold response – where sap flow decreased precipitously when soil moisture fell below a specific value. To exclude sap flow velocity measurements where water uptake is limited by the vapor pressure gradient, observations from the analysis where the relative humidity (a proxy for the vapor pressure gradient) was greater than 55 percent were excluded. The 55 percent relative humidity threshold was chosen from visual estimates of when the relative humidity effects overwhelmed the sap flow velocity signal. The relationship between

soil moisture and sap flow velocities during the summer and fall of 2015 (July 10th to November 1st) was analyzed at each tree.

Results

Time series of solar radiation, wind speed, wind direction, barometric pressure, rain, air temperature, relative humidity, and soil moisture and soil temperature are shown in Appendix 1. A depth profile time series of soil moisture is shown in Figure 6. Nearly a million records of soil moisture since November of 2013 have been collected at the study area. The summer dry-out and winter/spring wetting fronts are visible in at each site and depth. Coupled with the soil moisture measurements in Figure 6 are air temperature at the study area as well as precipitation data from the nearby NWS COOP station at Manzanita Lake. Air temperature tracks the dry out period while the effects of individual rain events are evident in the soil moisture profile time series.

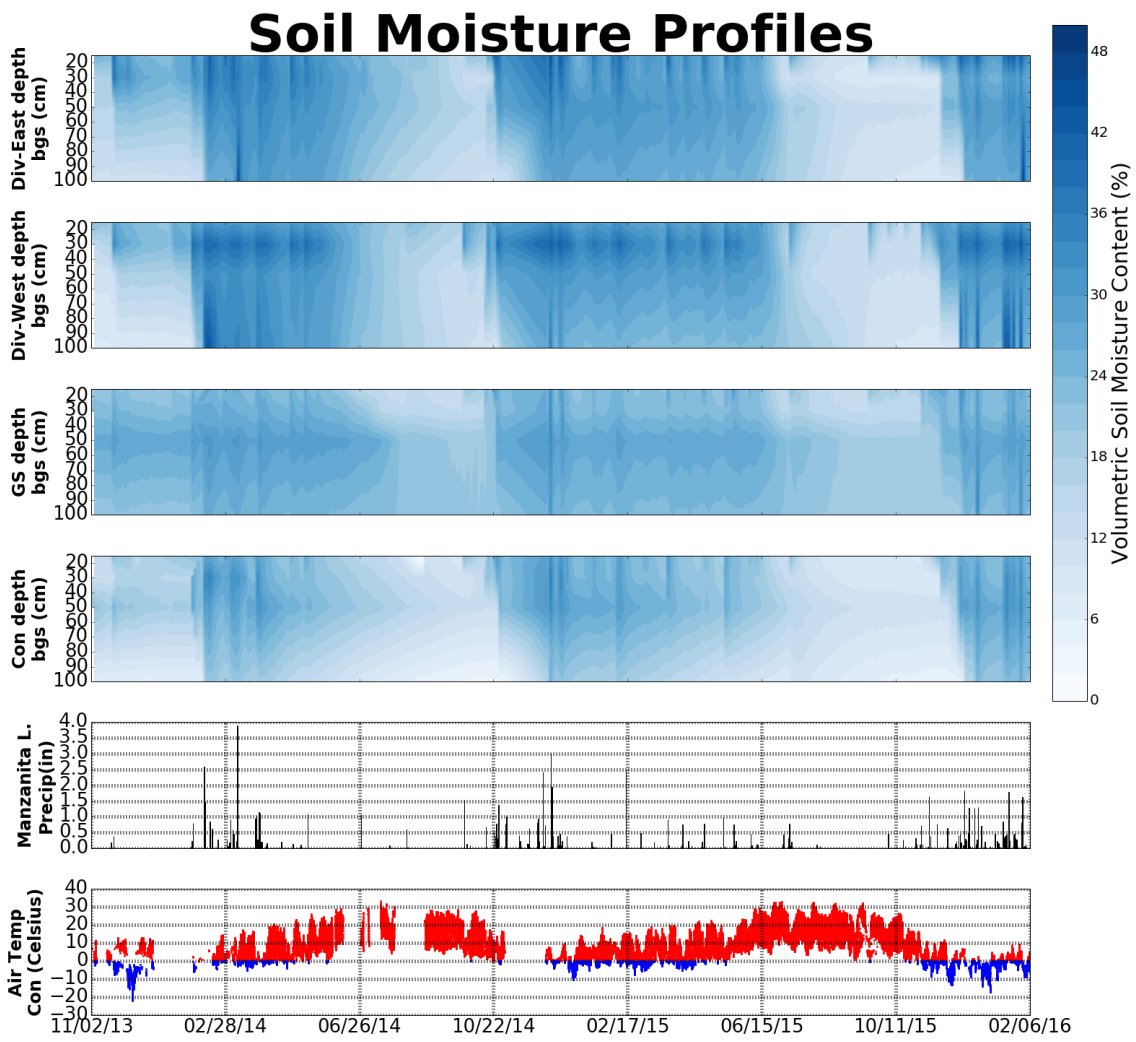

Figure 6: Soil moisture profiles are shown in the top four graphs from 15 to 100 cm bgs for each site. Dark blue indicates greater moisture levels while light blue to white indicates dryer soils. The nearby Western Regional Climate Center COOP station at Manzanita Lake precipitation time series and air temperature time series are shown in the bottom two graphs. Appendix 1 contains the= raw datasets used to interpolate the soil moisture profiles time series.

Analysis of the cumulative solar radiation is shown in Figure 7. The first column is the time series of solar radiation at each site. Nearly 250,000 measurements of solar radiation have been recorded since November of 2013. For days with a sufficient number of measurements, the solar radiative flux per day (mega joules per square meter) is shown in the second column. The red point indicate measured data while the blue points are calculated from linear

interpolation to fill the data gaps. The cumulative shortwave radiation from November 2013 is shown in the third column. Due to the thick forest canopy, the unmodified/control site receives the least amount of solar radiation at the ~2.5 meter height while the group select site receives the most solar energy, nearly 3 times the amount of the unmodified site. Note that the Div-West site has roughly the same cumulative energy flux as the unmodified site. This is attributed to the fact that the radiometer in the control was located in a small clearing that sees direct sun during the summer months. Therefore, the cumulative energy measurements at the unmodified site likely over-estimate the total energy that is indicative of the unmodified forest.

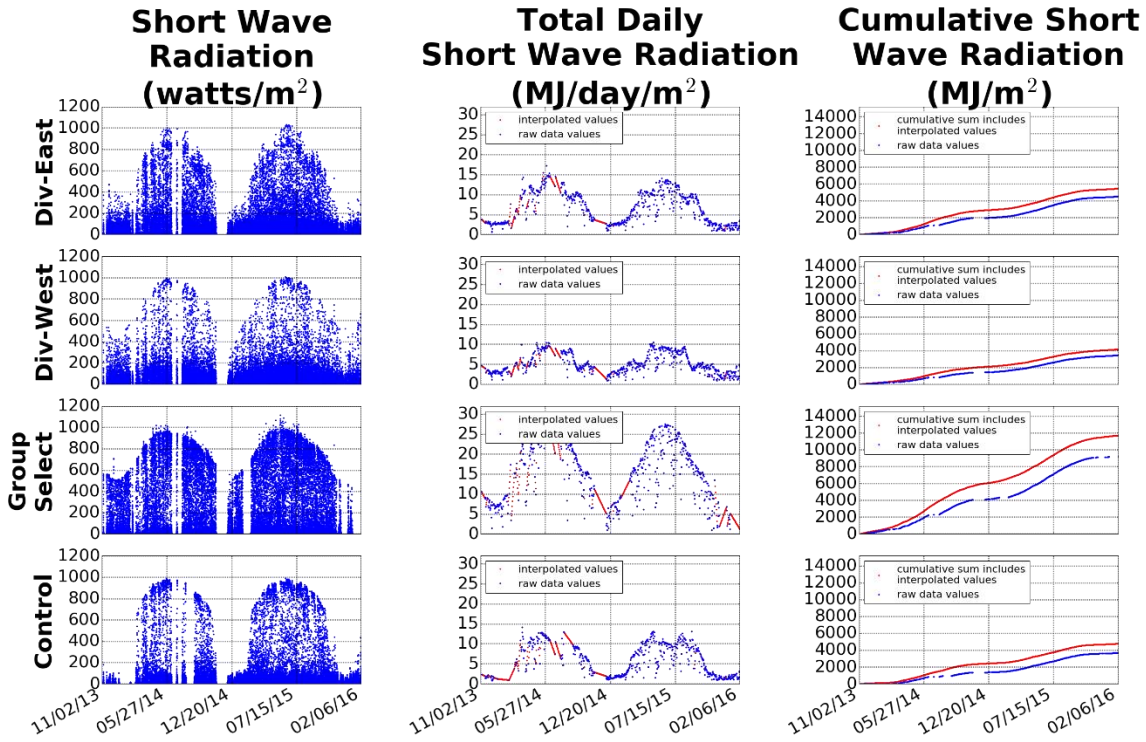

Figure 7: Measurements of incoming short wave radiation from the micro-meteorological towers are shown in column 1 graphs. Column 2 graphs are calculations of the total energy integrated over an entire day. Red points indicate days where missing records flagged the calculation as uncertain and therefore were interpolated from the blue observations. Column 3 graphs indicate the cumulative flux of cumulative shortwave radiation at each site. At the Group Select site, nearly 2 to 3 times more short wave energy is measured at the meteorological station than the other sites.

Results: Soil Moisture Dynamics

The time series of the daily average soil moisture at 15, 30 ,50, and 100 cm bgs for the four sites at the study area are shown in Figure 8. Soil moisture minimums at 100 cm bgs for 2014 and 2015 from July 1 to September 31 (roughly the recession/growing period) were lowest at the unmodified site (4.5% and 7.5%), near equal at the Div-West and Div-East sites (14.0 and 12.3, 14.9 and 14.3%), and highest at the Group Selection (21.1 and 19.5%). The elevated mid/late summer soil moisture at the Group Selection is the most pronounced difference between the four sites. This trend is likely due to the lack of deep rooted vegetation at the site relative to the other forested sites. However, the near surface (15 – 30 cm bgs) soil moisture measurements at the Group Selection do not exhibit elevated moisture content as seen at the 100 cm bgs depth. This is likely due to the abundant understory that has developed following the treatment and potential for bare soil evaporation.

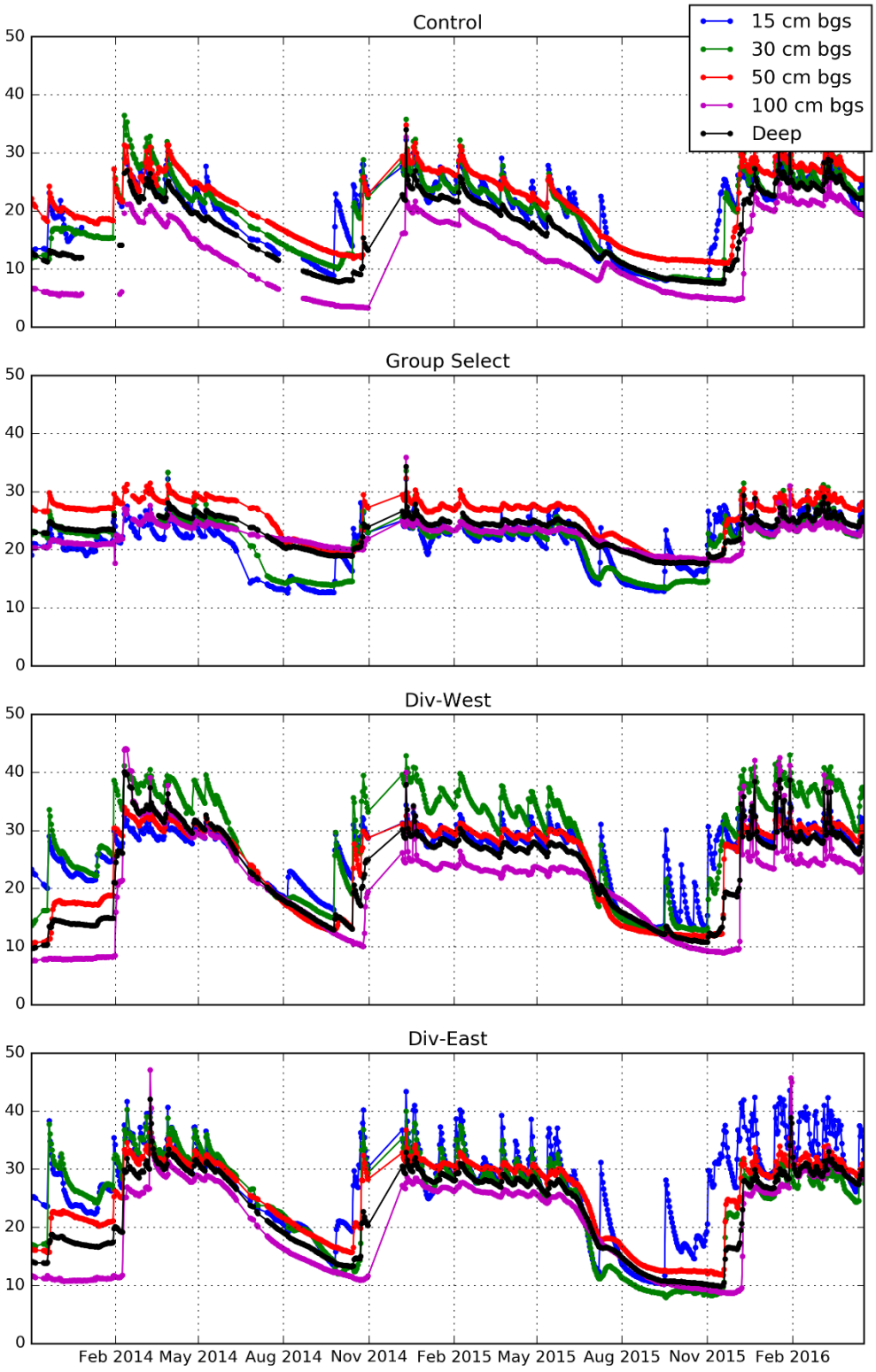

Figure 8: Time series of percent volumetric soil moisture at 15, 30, 50, 100, cm bgs as well as the integrated deep soil moisture metric at each site.

Figure 9 shows boxplots of the mean daily soil moisture from November 2013 to April of 2016 for each site at 15, 30, 50, 100 cm bgs, and the integrated deep soil moisture metric. In general, the unmodified site is drier than the managed sites. This observation is most pronounced at the 100 cm bgs depth. Furthermore, the spread/variance in the observed time series of soil moisture is substantially smaller at the Group Select site (quartiles and whiskers are more tightly clustered near the median). The reduced variance at the Group Select site is attributed to reduced transpiration which ultimately result in elevated soil moisture values at the end of the growing season, typically in the late summer or early fall.

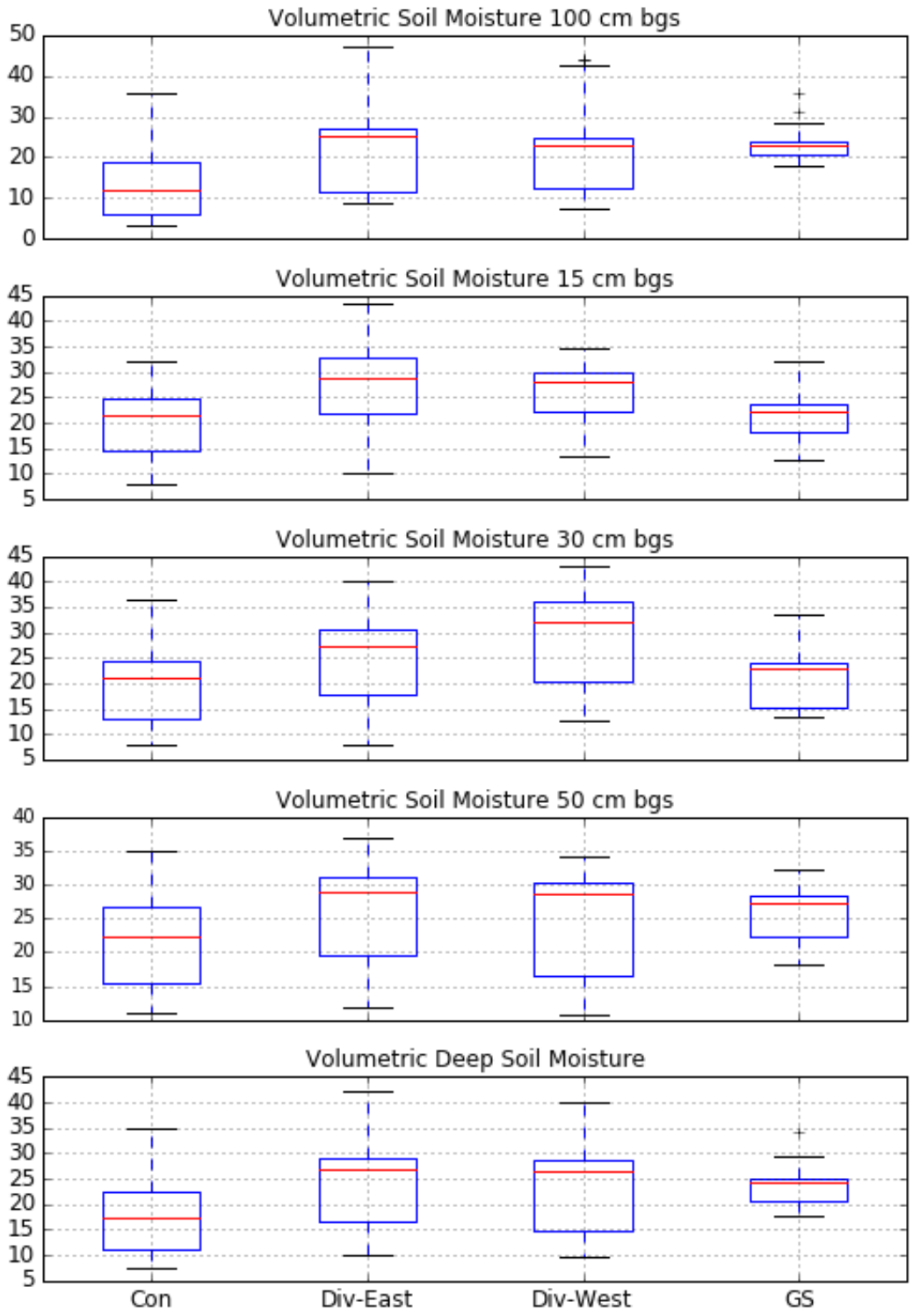

Figure 9: Boxplots of average daily soil moisture at each depth as well as the deep soil moisture metric for the entire record at each site. Boxes are drawn around the first and third quartiles, the red line indicates the median, and the whiskers extend to the minimum and maximum values.

To quantify the deep soil moisture dynamics the beginning of each soil moisture recession curve was calculated for the 2015 summer (Figure 10) and the recession equations were fit to the observations (Figure 11) at each site. The soil moisture recession at the unmodified site initiated the earliest in the year on March 29th, while the recession at the thinned sites began on June 12th and May 30th followed by the Group Selection on June 18th. The early recession at the unmodified site is not attributed to a shorter snow duration period because the 2014/2015 winter was snow-free excluding several small snowfalls that quickly melted out. Figure 12 illustrates a typical day during the 2014/2015 winter. Therefore, a possible explanation for unusually early recession and high variance in the soil moisture during the winter may be linked to the dense forest canopy at the control site. The canopy at the unmodified site will have the highest level of interception. Due to the lower than average level of precipitation during the 2014/2015 winter, interception would likely be a larger percentage of the precipitation budget than in normal precipitation years. Therefore, soils at the unmodified site were likely to see less water than the managed sites. However, Figure 8 shows the 15 cm bgs soil moisture sensor at the control site being recharged at the same time and magnitude as the other sites. Therefore, a reduction in the precipitation reaching the soil at the unmodified site does not seem to explain the early soil moisture recession.

An alternative explanation to the early recession of soil moisture at the unmodified site hinges on the strong evidence that the mid-winter energy balance is greater under the forest canopy than in the open at locations with average mid-winter temperatures greater than 2 ^{o}C (Lundquist et al., 2013). This energy regime results from the reduction in shortwave (solar) radiation, when moving from a clearing to beneath a canopy, is less than the corresponding increase in longwave radiation emanating from the forest canopy. Therefore, the PET at the

unmodified site is likely greater than that at the thinned or group selection and may result in increased bare soil evaporation and transpiration. To evaluate if the net radiation at the unmodified site is linked to increased transpiration, there should be a positive correlation between the rate of soil moisture recession and average daytime temperature (a proxy for the net energy). This approach assumes the primary flux of water out of the soils is a result of ET and that a continuity equation (Equation 7) holds valid. Figure 13 shows the relationship between average daytime temperature and the rate of soil moisture from the start of the unmodified soil moisture recession to the start of the recession at the modified sites (April to June). The daily soil moisture recession was at or below a rate of .35% per day, near to the resolution of the soil moisture sensors (.25%). However, because these values are daily averages, the effect of oversampling will increase the resolution of these instruments to much lower than the published resolution. The unmodified site exhibits the strongest relationship between temperature and the rate of soil moisture recession as well as the warmest average daytime temperatures. This finding indicates that, at the unmodified site, transpiration is occurring during the winter/spring at a rate greater than the modified sites.

Equation 7: $dSM/dt = -ET$

SM = Soil Moisture
T = time
ET = Evapotranspiration

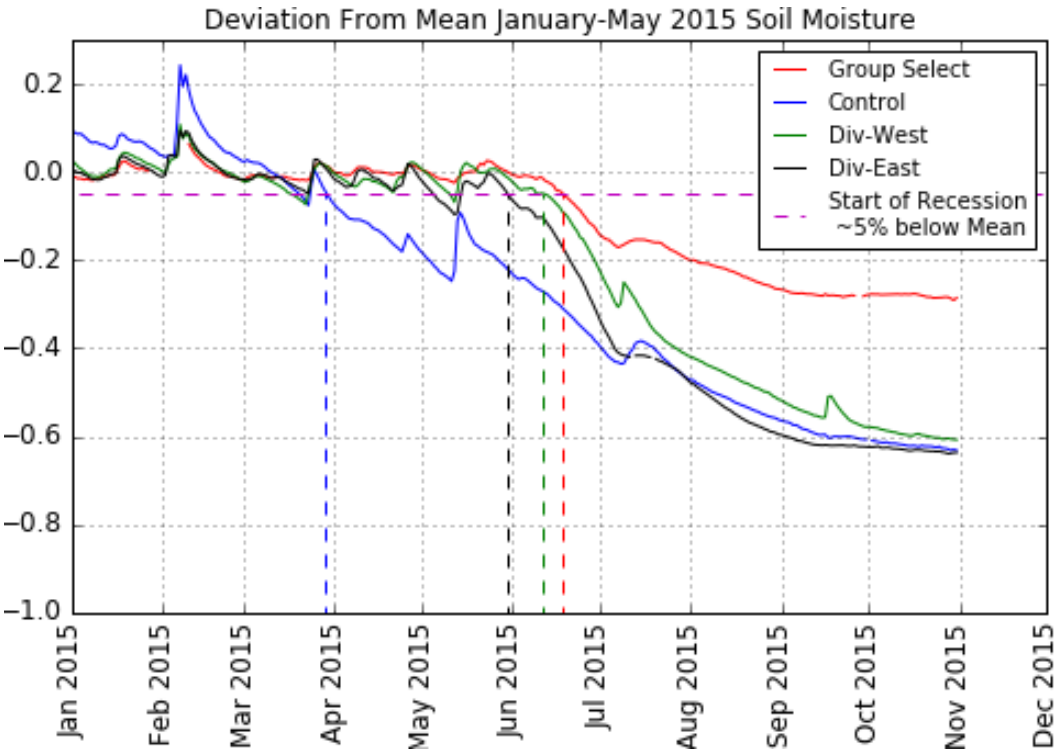

Figure 10: Percent deviation from the mean January to May 2015 deep soil moisture is shown for each site from January to December of 2015. The horizontal dashed line indicates the 5% below mean threshold. The last date that the soil moisture is above this threshold is defined as the initiation of the growing season recession. The date each site initiates the recession is indicated with vertically dashed lines.

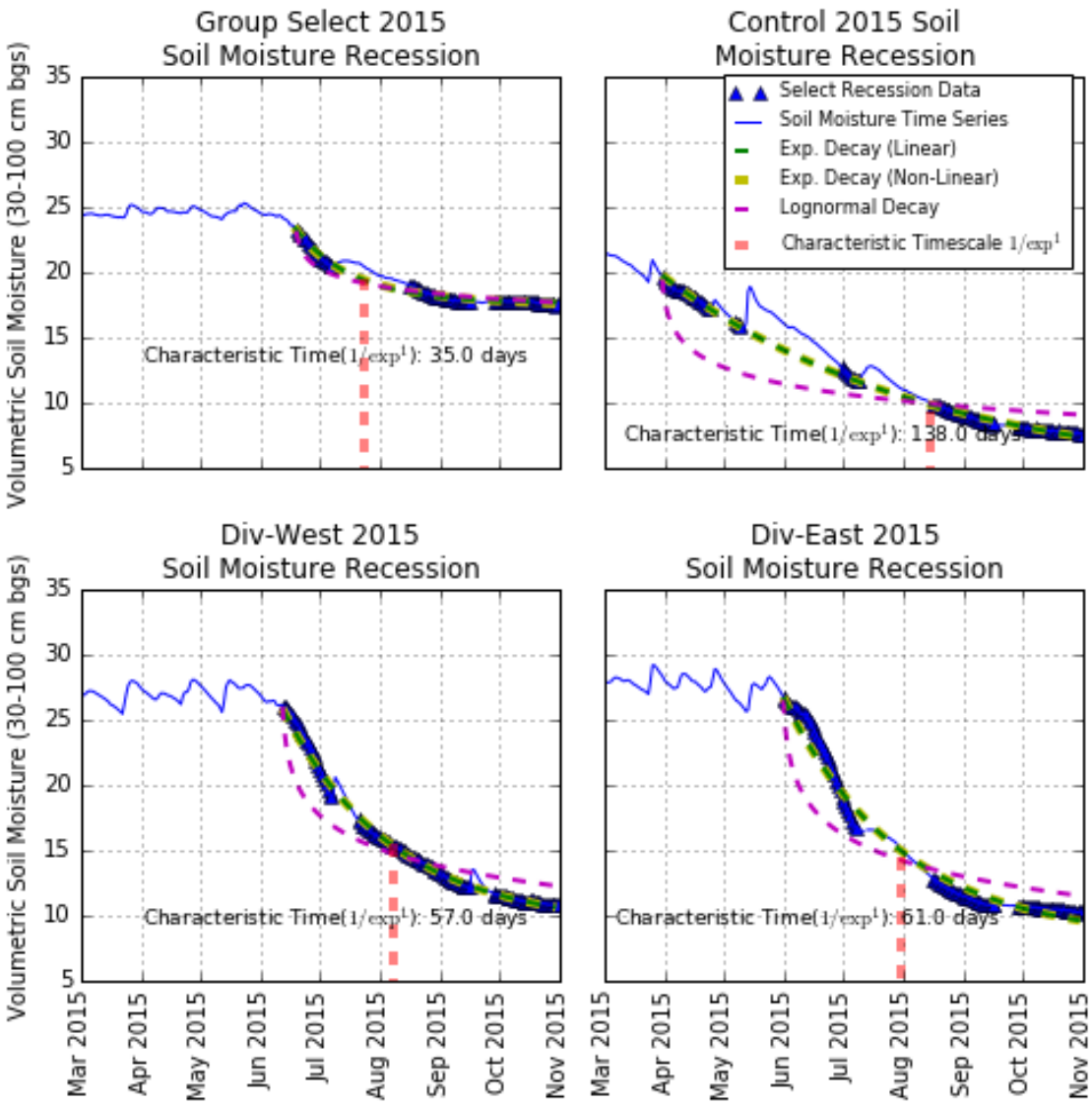

Figure 11: Deep soil moisture recession at each site. The blue line indicates the soil moisture time series from March to November of 2015. Blue triangles indicate the data used to fit the recession equations (Equations 4, 5, and 6). The fitted recession models are shown in green, yellow, and magenta. The characteristic time scale is shown in each graph with a vertical dashed red line.

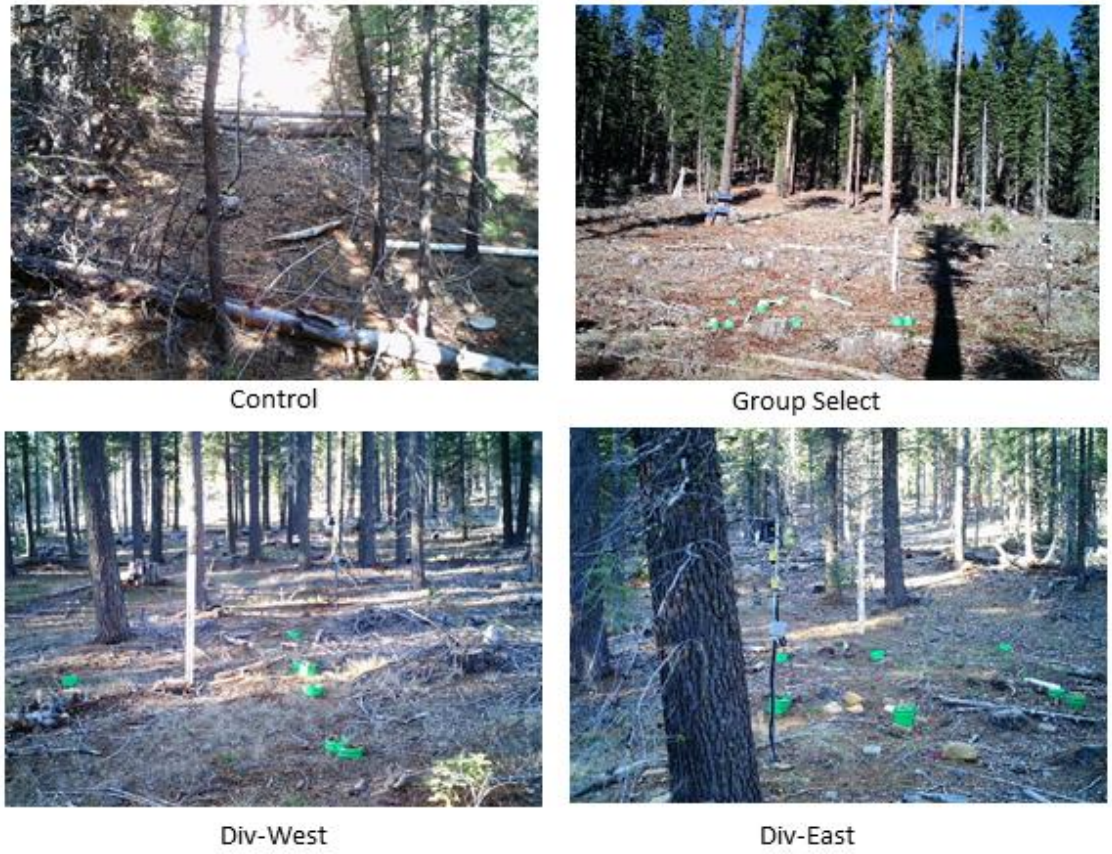

Figure 12: Pictures of each site on January 13th, 2015.

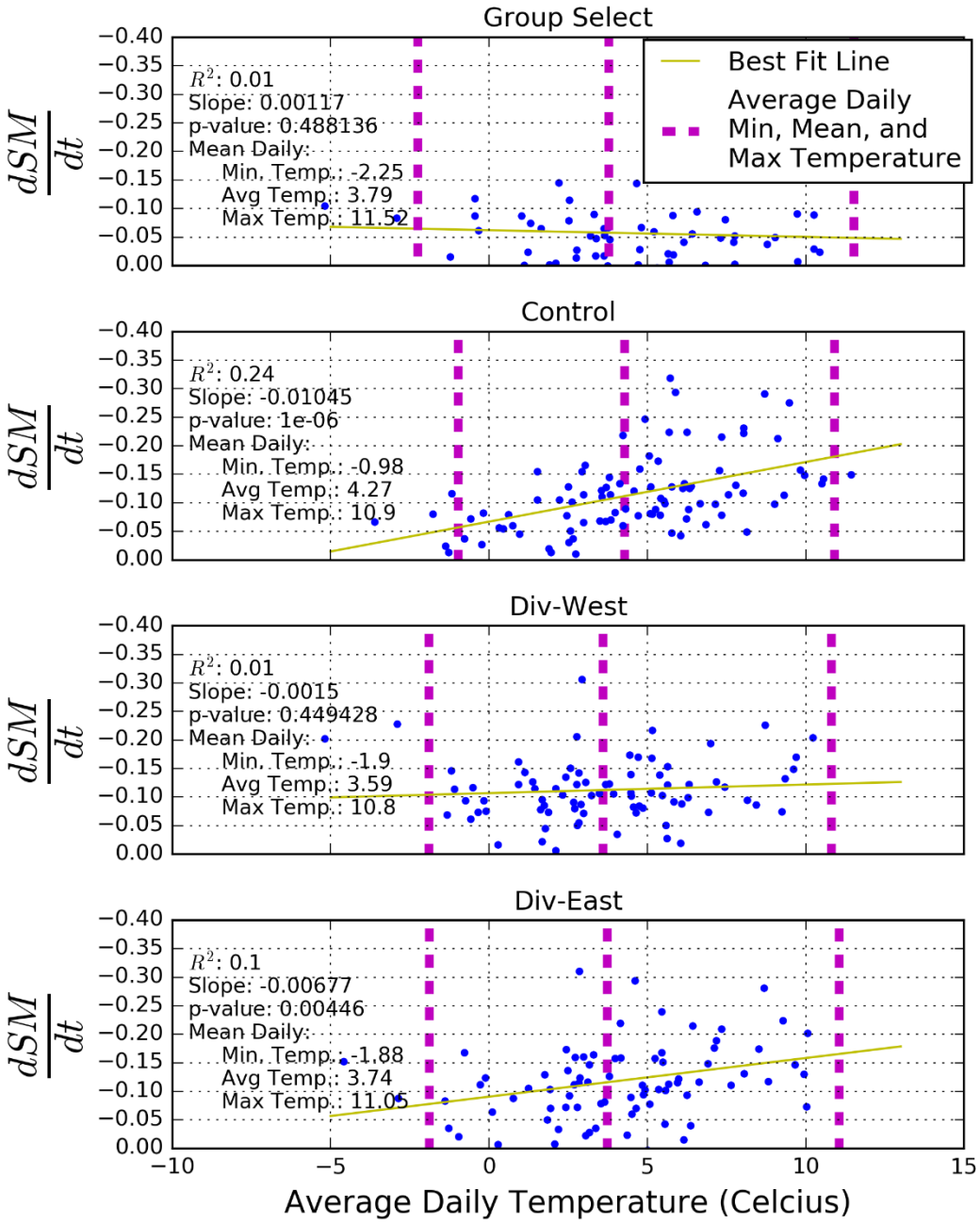

Figure 13: Daily soil moisture recession (dSM/dt) as a function of average daily temperature at each site from April 2015 to June 2015. The best fit line is shown in yellow along with the fit statistics. The average daily minimum, mean, and maximum temperatures are shown in vertically dashed magenta lines.

The observed minimum, maximum, and average temperatures at the study area from April to June of 2015 confirms the energy regime responsible for the earlier recession of soil moisture at the unmodified site. The Group Select site is warmest during the day as a result of direct solar radiation and coldest at night due to longwave radiation to the atmosphere. Meanwhile, the unmodified site is the warmest at night due to longwave radiation from the dense canopy (Figure 13). This dynamic results in the highest average temperatures at the unmodified site, suggesting that the net daily PET at the unmodified site is greater than at the managed sites during this time period.

The average daily minimum temperature at the unmodified site is substantially warmer (-.98 ^{o}C) than that of the modified sites (~-2 ^{o}C) (see Figure 13). The observed difference in the average daily minimum temperature at the study area suggests that there is a greater potential for energy use to convert water from liquid to solid in the modified sites than at the unmodified site. Therefore, this effect would be to dampen the observed differences in minimum temperatures between the sites as well as consume more energy at the modified sites by latent heating of water from a solid to liquid state during the day. Therefore, not only would the net energy be greater beneath the dense canopy at the unmodified site, a larger component of the net energy would be available for evapotranspiration rather than the phase change of solid to liquid water. The earlier initiation of soil moisture recession at the unmodified site can therefore be attributed to warmer temperatures, a greater net radiation budget, and an increase in PET that likely correspond to a higher rate of AET.

Of the equations to model the deep soil moisture recession (Equations 4, 5, and 6), the reservoir models are the best fit to the observations with coefficients of determination (r^2) values above .98. The logarithmic decay model had R2 values of .8, .73, .74, and .9 at the Div-

West, Div-East, Control, and Group Select sites respectively. Both the linear and non-linear models fit the data equally well. Therefore, because the linear model is less complex and most widely used, it was selected to characterize the recession of deep soil moisture at each site. The characteristic time scale of the recession at the unmodified, Div-West, Div-East, and Group Select sites occurred after 139, 55, 61, and 35 days respectively (Figure 11). The calendar date at which the characteristic time scale was reached (ie: ~63% of the recession was completed) for the unmodified, Div-West, Div-East, and Group Select sites was August 20th, August 6th, July 30th, and July 23th respectively. Considering the unmodified site initiated the recession curve much earlier than the other sites, it is surprising that it reaches the characteristic time later in the year than the other sites. A possible explanation may be that, due to the lower solar angle and ambient temperatures earlier in the year, the rate at which water may be extracted (i.e. AET) from the soil is much lower during the early recession period at the unmodified site relative to the early recession periods at the other sites. Therefore, the rate of soil moisture decline is generally much lower at the unmodified site than the thinned sites. Ultimately, as described by the soil moisture dynamics, the unmodified site appears to behave as an endmember with the earliest onset of the soil moisture recession, longest recession timescales, and lowest soil moisture values in the late summer/fall.

The soil moisture dynamics at the Group Select site are viewed as an opposing endmember to the unmodified site. The recession at the Group Select initiated latest in the year, the recession timescale was substantially shorter, and the subsequent soil moisture following the recession was much higher than the other sites. Conversely, the January – March 2015 deep soil moisture at the Group Select site was lower than the thinned sites. This may be a consequence of the absence of a canopy at the Group Select site. The removal of the canopy

may result in increased bare- ground evaporation and increased transpiration of near surface moisture from a dense network of shrub and grasses with shallow root systems. The bare ground evaporation and near surface transpiration increases are a result of an increase in net energy reaching the surface (no shading effects from the forest canopy – see Figure 7). Therefore, the ability to evaporate and transpire water at higher rates near the surface would reduce the amount of infiltration to soils at depth, resulting in a lower soil moisture contents in the deeper soils.

Results: Soil Moisture and Sap Flow Dynamics

Central to quantifying the forest structure – forest hydrology system is evaluating the limitations to forest transpiration. Excluding nutrient limitations and other secondary factors such as light, transpiration rates during the growing season at the study area are generally thought to be a function of available water and PET. As quantified by the Penman Monteith equation (Monteith, 1965), PET is a function of net energy and the vapor pressure gradient. Using the micrometeorological measurements of incoming solar radiation, wind speed, and relative humidity, both components of PET were either directly or indirectly quantified. To test how sap flow relates to soil moisture the mean day time (10 am to 4 pm) soil moisture was plotted against the mean day time sap flow velocity from July 10th 2015 to November 1st 2015 in Figure 14. The micrometeorological measurements in the Group Selection were applied to both the Tree 1 (seed tree) and the tree along the Group Select - thinned boundary (edge tree) while the micrometeorological measurements at the Div-West site were applied to Tree 4 located in the thinned forest. A confounding factor in de-convolving the sap flow – soil moisture relationship is the strong effect vapor pressure deficit can have on PET and sap flow. To control

for this effect, all data points were the relative humidity is greater than 55 percent were removed. The resulting relationships are shown in Figure 14.

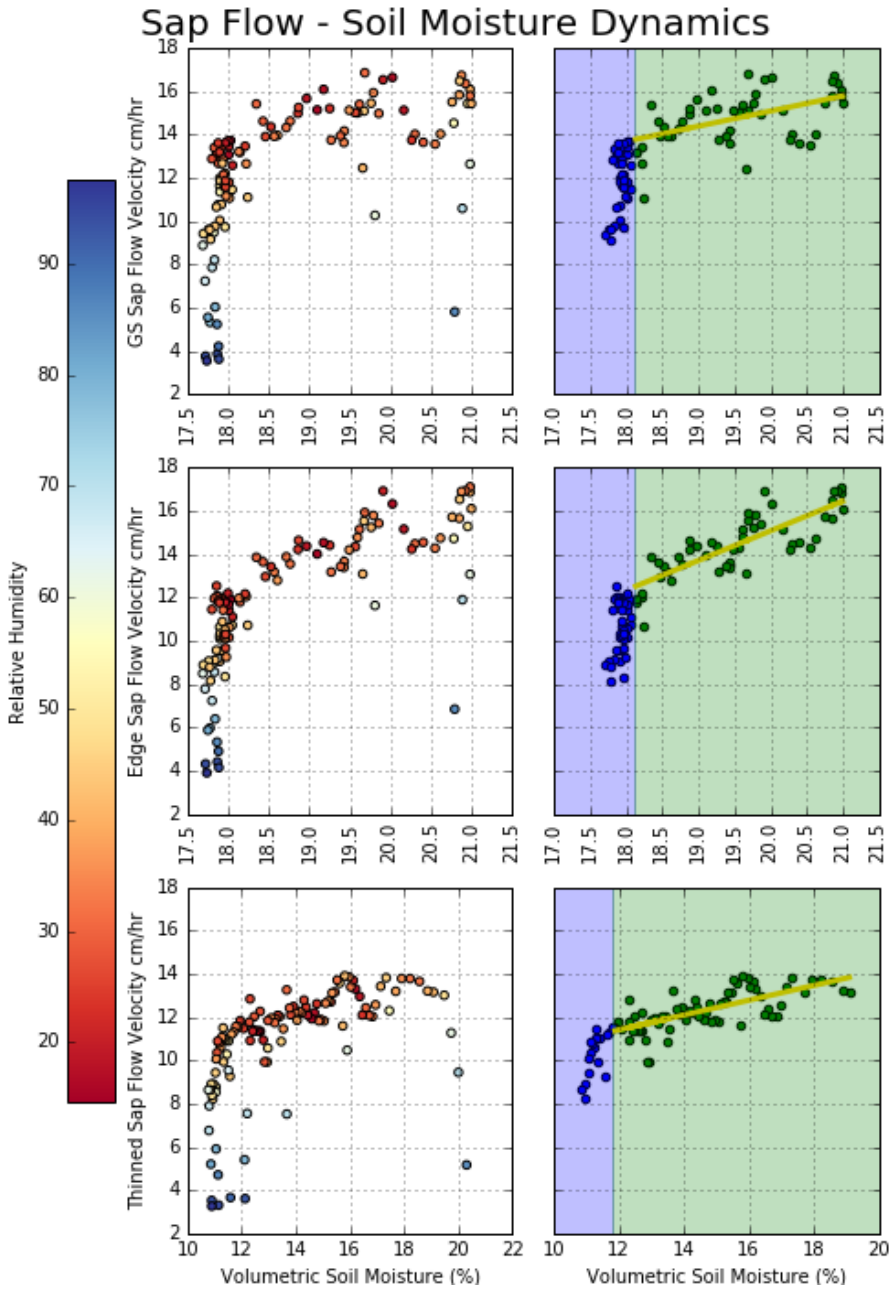

Figure 14: Sap flow versus soil moisture for tree 1 (Group Select), tree 2 (Edge Tree), and tree 4 (Thinned tree). Column one observations are colored with the relative humidity (0 – 100 %). Column 2 graphs remove all measurements with relative humidity values above 55%. Green observations represent sap flow measurements above the threshold value while blue points indicate points below the threshold values.

The soil moisture - sap flow relationship appear to be near-linear (green shaded area in Figure 14) with increasing sap velocity and soil moisture for much of the soil moisture range. This suggests that, since July 10th 2015, the forest transpiration rates were strongly water limited. However, because the Group Select micrometeorological measurements are not spatially coincident with the seed tree or edge tree, the absolute value of the soil moisture measurements experienced by the seed and edge tree is likely substantially different than that measured at the Group Select micrometeorological site. It is likely that, within the root system of the seed and edge tree, the soil moisture is drawn down to much lower values than at the Group Select soil moisture measurements. This is evident in the range of soil moisture values for the edge and seed trees versus the range in soil moisture values for the thinned tree. However, due to the well-established nature of spatial stability exhibited by soil moisture, it is defensible to translate the soil moisture dynamics from the Group Select micrometeorological measurements to the soil moisture dynamics as experienced by the seed and edge trees.

The historic drought severity during the study period provided a unique opportunity to look for threshold response to low soil moisture values. From Figure 14, the linear relationship shown in the green shaded region breaks down at low soil moisture values in the blue shaded region. This apparent threshold response to low soil moisture values is likely a function of the trees inability to overcome the capillary forces retaining water within the soils. The threshold is reached at the three trees at values of 18.1 and 11.5 percent volumetric water content at the Seed and Edge tree and the thinned tree, respectively. As discussed previously, the soil moisture value is probably substantially lower than the 18.1 percent value measured at the micrometeorological station within the Group Select treatment. It is important to note that this

is the depth of the average soil moisture value. Therefore, a percentage of the soil profile may still be above the threshold response but the co-located roots are not able to extract enough moisture to meet the evaporative demand. Once this threshold is reached, trees are forced to close their stomata's, cease photosynthesizing, and are forced to draw resources from strategic reserves. If low soil moisture conditions persist, trees risk extending into a state of carbon starvation and eventually mortality. Therefore, quantifying this threshold for forests is a critical environmental metric for better understanding the susceptibility of forests to persistent droughts.

The threshold response found in Figure 14 was applied to the Group Select and Div-West time series of deep soil moisture (Figure 15) for the period of record to examine the frequency and duration the two sites were at or below the threshold values. Considering that the 2014 water year had substantially less precipitation than 2015 (Figure 4), it was predicted that the soil moisture levels during the 2014 growing period would be equivalent or below the 2015 levels. However, due to the higher temperatures in 2015 and cumulative effects of drought (Figure 4 and 5), the soil moisture minimum during the 2014 growing period were slightly higher than the 2015 period and neither the Group Select nor Div-West soil moisture reached the threshold values during 2014 recession (Figure 15).

Due to the limited sample size (three trees), and study duration (one year of coincident sap flow – soil moisture data), it is problematic to extrapolate the soil moisture – sap flow results beyond the Ponderosa Pine species, geographic area, physiographic characteristics, and study interval. Even so, this data suggests the water stress in the forest was more severe during the 2015 growing season than the 2014 growing season. Consequently, it is reasonable to speculate that the broader forest in the study area did not experienced stomatal closure during

the 2014 growing season but may have during the 2015 growing season as a consequence of soil moisture levels.

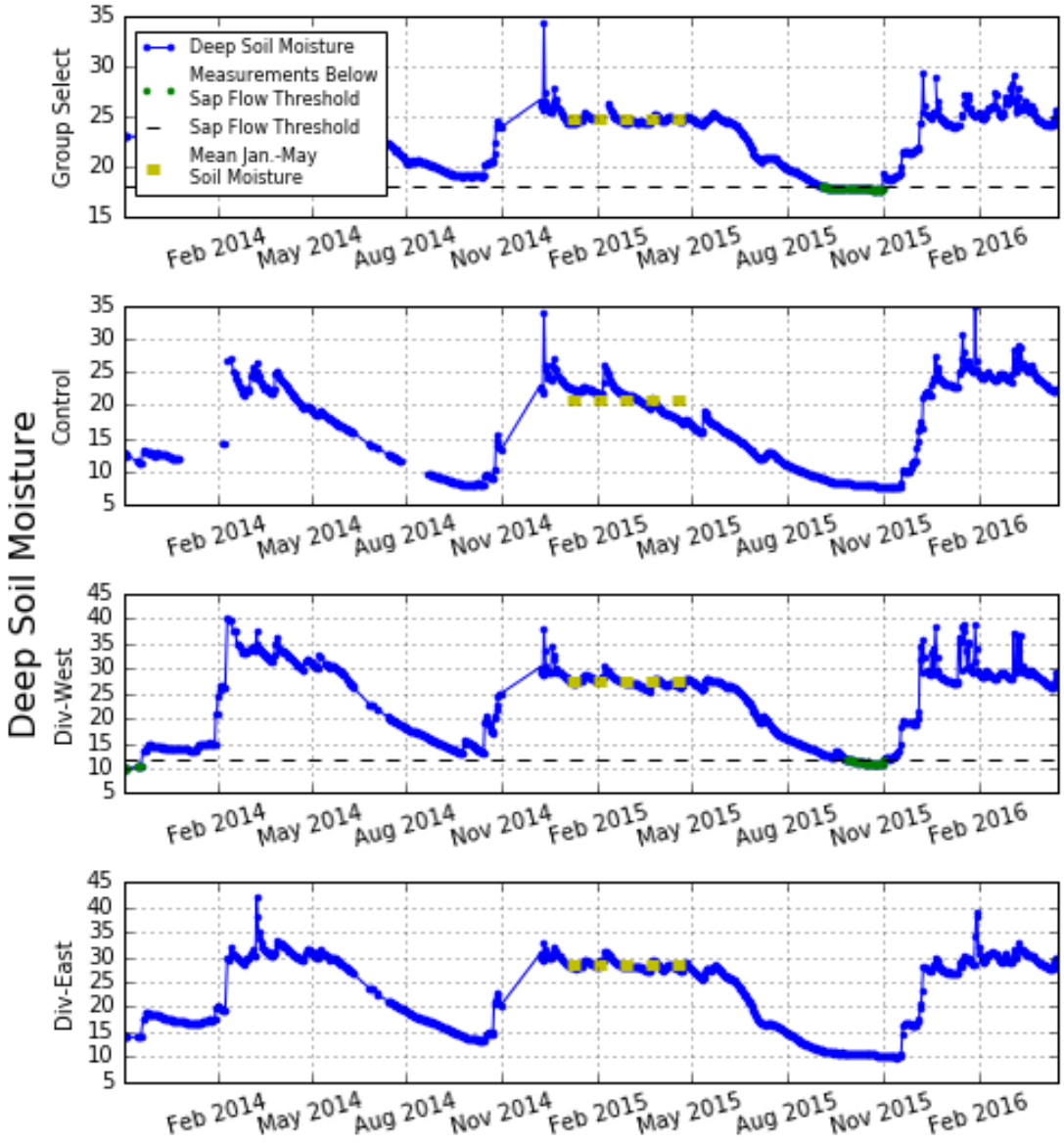

Figure 15: Time series of the deep soil moisture metric for each site. Dashed yellow lines indicate the January to May mean soil moisture metric calculated in Figure 4. The green dashed lines on the Group Select and Div-West time series indicates the sap flow soil moisture threshold. The green points on the Group Select and Div-West time series indicate measurements at or below the sap flow - soil moisture threshold

These results indicate that, for large, healthy, and mature Ponderosa Pines, it was not until the fourth year of the historically severe drought that they reached soil moisture levels that were capable of causing stomatal closure and severe stress (McDowell et al., 2008). Therefore, considering the historic nature of the current drought, it appears that these trees are well-adapted for the range in the historical distribution of droughts (Bales et al., 2015). However, this also indicates that the anomalous nature of the current drought reached a magnitude that was outside the adaptation range for these trees and was capable of transitioning them to the initial stages of carbon starvation. While there is a high level of uncertainty in precipitation regimes across the northern Sierra Nevada, the increased temperatures, and decreased snow duration are likely to produce a higher frequency and more severe drought conditions. As such, there may be a level of susceptibility of forests in Lassen National Forest to future droughts that has the potential to degrade the overall health of the forests.

The multiple linear regression model used daily (10AM to 6PM) average values of relatively humidity, wind speed, solar radiation, and deep soil moisture was able to predict the sap flow velocity data exceptionally well (Figure 16). For the three trees instrumented with sap flow sensors (Group Select, Edge, and Thinned) all four dependent variables were found to be significant at or below a p-value of .1. The statistical model was able to fit the observed mean daytime sap flow velocities with a r-square of .89, .91, and .85 at the Group Select, Edge and Diversity Thinned tree, respectively (Figure 16). The strong fits between the modeled and observed data indicate that this approach may be an extremely valuable method for quantifying canopy transpiration dynamics in similar forested landscapes.

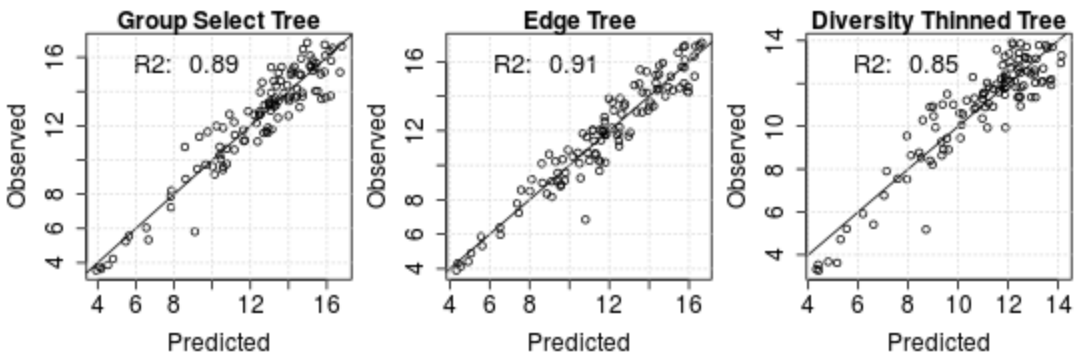

Figure 16: Fit results for the multiple linear regression model of predicted versus observed sap flow velocities. The model uses soil moisture, incoming solar radiation, wind speed, and humidity to predict sap flow. All predictor variables were found to be significant. The model r^2 for each tree is shown in each graph.

Using the linear regression model, the relationship between soil moisture, humidity, wind speed, and solar radiation to sap flow velocities was deconvolved (Figure 17). The strongest relationships at the three trees in Figure 17 are deep soil moisture and relative humidity followed by solar radiation and wind speed. These results indicate that, from the start of the measurements (July 10th, 2015), the transpiration at all three trees were in a state of water limitation, rather than energy limited. To better quantify the relative magnitude of water limitation at the three sites, the linear model was implemented in a predictive capacity. The relative humidity, wind speed, and solar radiation values were held constant at the mean of daily average values of the modeling period (July 10th to November 1st, 2015) and the time series of deep soil moisture values were applied to the model. The relative sap flow velocity reductions as a function of the soil moisture time series throughout the modeling period are shown in Figure 18. Excluding a minor increase in sap flow velocities at the Group Select and Edge trees, the three trees initially decrease at relatively similar rates. However, around day of year 210 (July 29th, 2015), the rate in reduction at the Diversity Thinned tree decreases substantially relative to the Group Select and Edge trees. The rate in reduction of sap flow velocities at both

the Edge and Group Select trees abruptly reach zero near day of year 255 (September 12th, 2015). Following day of year 255, both the Edge and Group Select trees maintain a daily average sap flow velocity at roughly 70 and 80 percent there initial (July 10th, 2015) rates, respectively. The Diversity Thinned tree experiences a much more gradual rate in reduction of sap flow velocities relative to the Group Select and Edge trees. Furthermore, a precipitation event around day of year 260 (September 17th, 2015) infiltrated to the deep soils (30-100 cm bgs depth interval) at the Diversity Thinned site, but did not penetrate the deep soil layers at Group Select site. As a result of the increased infiltration to deep soils and the slower rate of sap flow velocity reduction, the Diversity Thinned maintained a much greater relative sap flow velocity into the summer and fall to nearly day of year 275 (October 2nd, 2015). Furthermore, the Diversity Thinned site did not reach a point at which the relative sap flow velocity was unchanging as opposed to the Group Select and Edge sites.

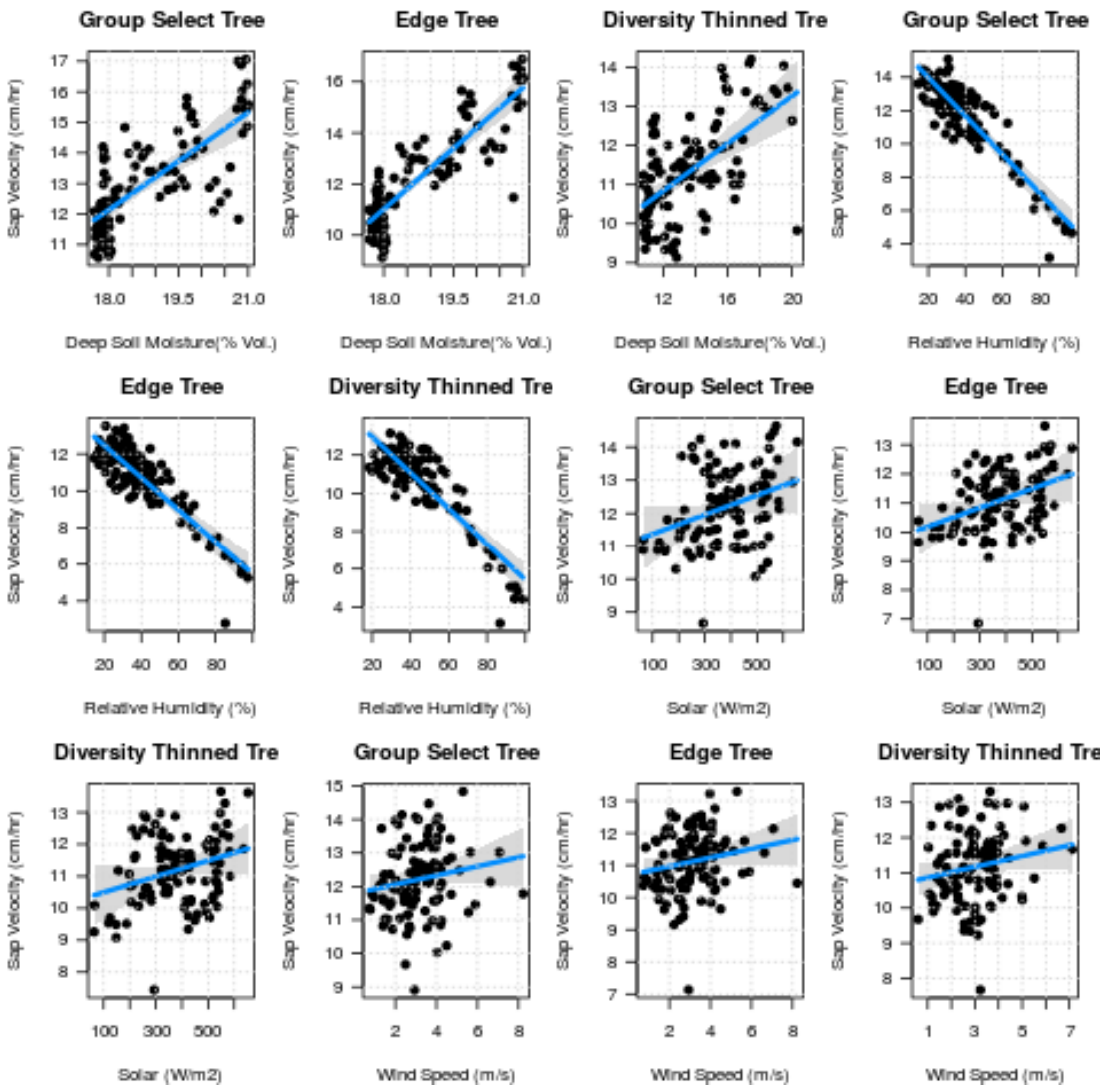

Figure 17: Visualization of the regression model for each predictor variable are shown for each tree. The best fit model (blue line) and confidence interval (shaded region) are shown in each graph.

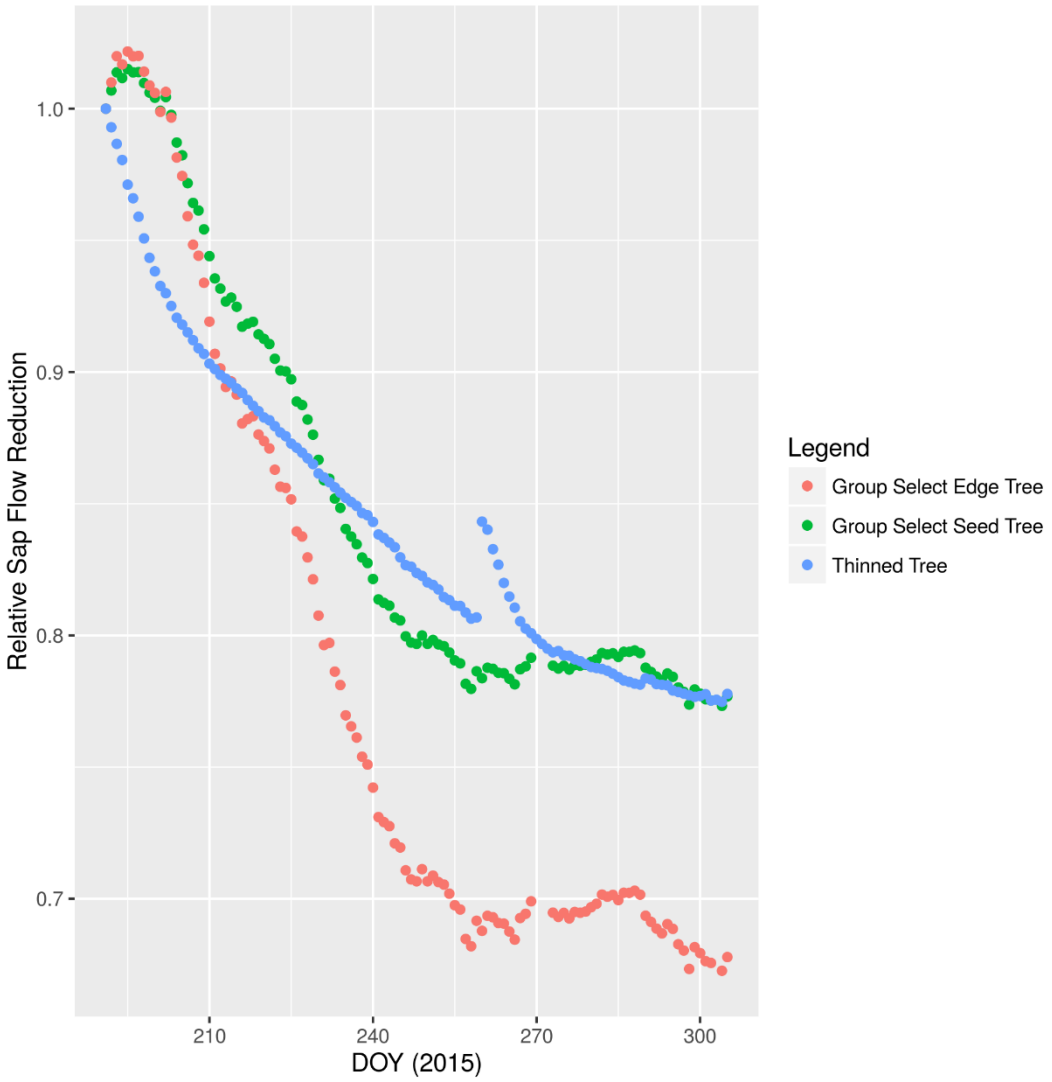

Figure 18: Reduction in sap flow velocities as a function of the deep soil moisture time series at each tree.

Discussion

Forest resilience to climate change and the subsequent heightened prevalence of wildland fire and infestation is a pressing concern facing land managers and communities across the Western United States. In response to increased risks to forest, forest management strategies and fuel reduction treatments are widely implement to improve forest health.

However, critical to the effectiveness of these approaches is to better quantify how stand density, canopy properties, and fuel reductions may impact forest hydrology, specifically soil moisture dynamics. This research provides a site-specific study of soil moisture dynamics and tree health across two forest management strategies, thinning and group selection during an unusually severe drought.

The soil moisture dynamics are markedly different across the unmodified, Group Select, and thinned sites. Concurrent with the stand and canopy density at each site, the unmodified site acts as a soil moisture end member while the group selection site acts as the opposing endmember. The substantially earlier initiation of the soil moisture recession at the unmodified site is an important observation of this study. As a result, the unmodified site reached the lowest level of soil moisture in 2015 and consistently had lower levels of moisture than any of the other treated sites. The early recession at the unmodified site is likely a function of the denser canopy resulting in increased net energy at the forest floor. The effects of the dense canopy in the unmodified forest suggest that the vegetation will reach a more severe stress condition, earlier in the summer than at the modified sites.

The soil moisture recession dynamics at each site were directly related to the ability of vegetation to extract water from the soils. The elevated moisture content at the Group Select site into the summer/fall is a result of reduced root access to deep soils. Furthermore, based on the recession characteristics (such as the characteristic time scales), it is likely that increased temperatures and longer growing seasons will increase forest water stress. Due to the reduced canopy density, the thinned site soil moisture recession was initiated near the same time as the Group Select recession. However, as the growing season progressed, the soil moisture dynamics at the thinned sites more closely resembled the soil moisture trends in the unmodified forest.

The bimodal nature of the thinned forests suggests that the reduced canopy was able to delay the soil moisture recession until later in the season and that the forest was able to access the full extent of the subsurface moisture late into the summer and fall. Therefore, developing a more nuanced assessment of the ideal forest canopy density/structure that may delay the onset of the soil moisture recession is of critical importance to developing forest management strategies to improve forest health.

Sap velocity data collected at three trees across the study area was critical to quantifying the relationship between soil moisture and tree health. Due to the unprecedented nature of the drought during this study, the adaptation range of ponderosa pines to low soil moisture levels was better quantified at the study area. The instrumented trees appeared to reach soil moisture levels that led to stomatal closure during the 2015 growing season. Counter-intuitively, the Group Select and Edge trees appeared more vulnerable to the soil moisture reduction during the growing season. The Group Select treatment had lower winter and spring soil moisture than the unmodified site. This is likely due to reduced infiltration as a result of increased understory transpiration that prevented the soils in these locations from being recharged during the late spring/summer. Even though the observed soil moisture values at the Group Select site were higher than the other sites in the summer/fall on average, the soil moisture around the seed and edge tree root networks were likely substantially lower. Coupled with the reduced soil moisture during the winter and spring, there are indications that that seed trees within the Group Selection treatment may be more vulnerable to water stress during prolonged droughts than the trees in the thinned forests.

Overall, these findings suggest that there is a distinct trade-off between high density forests and cleared areas. Cleared areas have higher soil moisture later into the growing season

yet the trees in these clearings may be more susceptible to drought stress. Conversely, high density forests initiate the soil moisture recession earlier in the season and are likely to have far dryer soils at the end of the growing season. Therefore, defining the ideal forest density that will maximize the benefits of both these attributes is critical to developing a management strategy to promote drought resilient forests.

As illustrated in this study, quantifying the ecologic and hydrologic interactions and interplay is fundamental to future improvements to forest management to develop climate change adaptation strategies for western forests. This study provides insights to two common management strategies in Lassen National Forest. However, the scope of this study makes it challenging to extrapolate the results across the entire Lassen National Forest landscape with differing physiographic characteristics. Therefore, more work needs to be conducted to develop better mechanistic approaches to represent forests in distributed hydrologic modeling. This will require larger site level studies implementing replication across a variety of physiographic and vegetation assemblages.

Chapter 2: Relating Space-Based Estimates of Total Water Storage to Hydraulic Groundwater Theory: Implication for Sierra Nevada Low Flows in a Warming Climate

Introduction

Projected increases in prolonged drought events due to climate change may strongly alter ecological dynamics and water resource security. For much of California and Nevada, water resources are heavily dependent upon the Sierra Nevada Mountain snow pack and stream flow. Highlighting this relationship, the current five year prolonged drought event across much of the western United States has drastically reduced annual snow packs and stream flows and has seriously stressed water resources. These reductions in stream flows are closely tied to ecosystem health, industrial and agricultural vitality, and community sustainability. Due to the difficulty in predicting the long-term impact of climate change on Sierra Nevada Mountain hydrology (Cayan et al., 2008; Dettinger et al., 2004; Leung et al., 2004), there are many uncertainties surrounding how stream flow regimes may be altered in the future.

Of particular importance within the stream flow regime is the distribution of stream low flows. Annual stream low flows are critical to ecosystem health and are an essential source of late season water supply to water resources. Traditional statistical methods that use historical data to characterize low flow regimes generally rely on the assumption of stationarity. Due to the apparent modification/intensification of the hydroclimatic system as a result of climate change, the assumption of stationarity is problematic (Pal et al., 2015; P. C. D. Milly et al., 2008). Disentangling the climatic signal from historical variability of stream flow time series is further complicated by hydrogeological factors that can have a significant role in mediating the hydrologic response to climate change (Tague et al., 2008). For instance, Tague and Grant (2009) found that, a 1.5 °C warming scenario for a slow draining watershed would result in four times

the reduction in stream low flows than for a fast draining watershed. This finding illustrates the importance of analyzing lows flow dynamics within a geo-climatic framework.

Due to the dry hot summers associated with the Mediterranean climate of the Sierra Nevada and the strong topographic relief in most headwater catchments, low flows are generally considered to be derived from subsurface groundwater storage. This conceptual model assumes subsurface water is recharged during spring snow melt and is gradually depleted through the summer as it drains through the subsurface. Hence, annual changes in summer/fall low flows are considered a direct result of the changes in subsurface water storage (Smakhtin, 2001).

Quantifying the relationship between subsurface water storage and streamflow is challenging due to the spatial complexity and heterogeneity of the subsurface and stream flows in space and time (McNamara et al., 2011). Point measurements of storage from wells are insufficient to characterize the storage across a catchment in mountainous environments with complex geology. This study presents a novel approach to quantify the storage-flow relationship using space-based measurement of storage from NASA's Gravity Recovery and Climate Experiment (GRACE) satellite for 10 gages in the Hydro-Climatic Data Network (HCDN) located in the Sierra Nevada. The specific objectives were to: 1.) Test if the large-footprint Space-based measurements of Total Water Storage Anomalies (TWSA) from the GRACE satellite are well correlated to Sierra Nevada low flows; 2.) Predict how storage capacity, as defined by the catchment geology, may mediate or exacerbate the hydro-climate signal as seen in stream low flows in mountainous catchment; 3.) Compare the storage-discharge dynamics from space-based measurements of storage to that predicted by hydraulic groundwater theory (HGT). It was predicted that the magnitude of annual stream low flows are a good measurement of

catchment scale storage and will be well correlated to space based measurements of total water storage. However, due to the spatial mismatch between the storage and flow measurement and theoretical assumptions within HGT, the observed storage – flow relationship may not align precisely with the predictions of HGT.

Methods: Data Compilations

Daily unimpaired stream flow data across the Sierra Nevada was acquired at 12 USGS HCDN stream gages. The USGS HCDN dataset (Slack, J.R. and Landwehr, 1992) was selected because it measures flows in catchments that are unimpaired by upstream diversions and are able to capture the hydrologic response to climatic fluctuations. A total of 12 gages with data during the study period from 2002 to 2015 and a minimum of 300 daily measurements per year were selected. Two of the gages consistently reached no-flow conditions and therefore were excluded from the analysis. The resulting 10 gages and catchments are shown in Figure 19. For each stream gage in the study, catchment characteristics were derived from the USGS Stream Stats database. Table 1 lists the catchment characteristics and published low-flow observations for each of the 10 catchments. To assess low flows, the seven day rolling average annual low flow, hence forth denoted as Y_7 (also known as the drought flow) normalized by catchment area (Brutsaert and Sugita, 2008), was used. Y_7 is used in this study because it is a good representation of a storage-derived flow and has been widely utilized in drought flow studies throughout the literature.

Gage	Drainage Area (mi^2)	Main Channel Length (mi)	Stream Slope (ft/mi)	Percent Forest	7 Day 20 Yr Low Flow (ft^3/sec)	Extrusive (%)	Unconsolidated (%)	Intrusive (%)
10308200	276	30.8	104	100	-	60.4	0	38.3
10343500	10.5	4.9	381	57.6	1.1	56.8	43.2	0
11230500	52.5	14.3	325.4	10.8	2.3	7.3	5.4	85
11237500	22.9	7.7	247	43.3	0.1	0	17.3	82.6
11264500	181	19.8	144	66	2	4.7	15.1	79.9
11266500	321	28.6	235	70	10.7	2.7	18.1	78.7
11315000	21	10.5	228	37.7	0.1	10.1	8.3	81.6
11381500	131	50.9	115	36.7	66.1	97.7	0	0
11383500	208	54.6	104	54	57.9	98.7	0.7	0
11427700	9.9	5	142	65.4	-	71.5	0	0

Table 1: Basin Characteristics. High storage capacity basins are highlighted in blue and low storage capacity basins are highlighted in light pink.

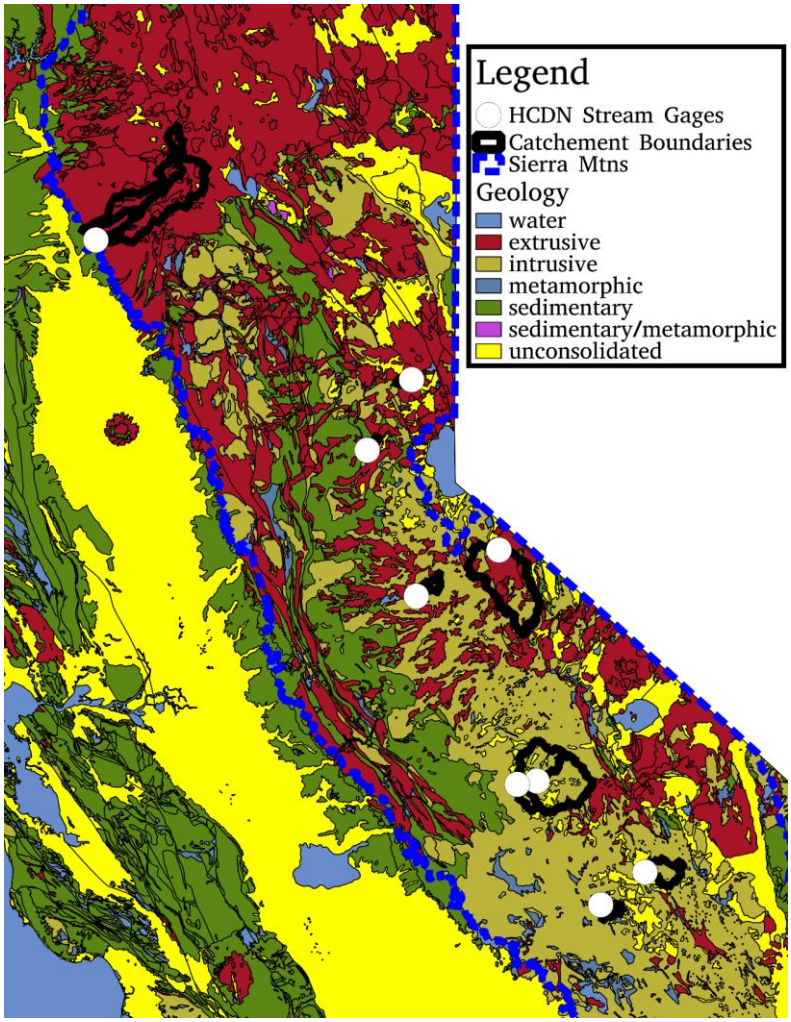

Figure 9: Overview map of study area showing the ten catchments, HCDN gages, and geologic interpretations. The dashed blue line roughly outlines the Sierra Nevada.

Catchment-scale measurements of storage in mountainous terrain are difficult to quantify, as previously highlighted. Therefore, rather than using the traditional estimates of storage derived from sparse well networks, the Gravity Recovery and Climate Experiment (GRACE) satellite was selected to estimate the catchment storage at the 10 HCDN gages. The GRACE Monthly Land Mass Grids dataset was acquired through the Jet Propulsion Laboratory (ftp://podaac-ftp.jpl.nasa.gov/allData/tellus/L3/land_mass/RL05/geotiff/). The GRACE measurements were processed using RL05 spherical harmonics from the University of Texas at Austin Center for Space Research and a 300 km filtering and de-stripping algorithm (Swenson, 2011, 2002; Swenson et al., 2008). Following processing, the dataset is distributed as a 1 degree gridded dataset of monthly measurements of Total Water Storage Anomaly (TWSA). While the dataset is distributed in 1 degree gridded measurements, the actual footprint of each pixel value is substantially greater than that of pixel area. The TWSA is a measurement of monthly changes in total terrestrial water storage relative to the 2004-2009 average. GRACE measures mass anomalies across the entire terrestrial hydrologic profile.

A significant challenge and methodological pitfall to apply the GRACE TWSA dataset to the study catchments is the mismatch in the spatial scales between the two datasets. However, the traditional approach to derive estimates of catchment storage from well measurements may have a greater spatial mismatch than the satellite derived measurements. The average drainage area of a catchment in the study is 319.5 km^2 and ranged from 25 to 831 km^2. Therefore, the GRACE measurement footprint (300 km radius Gaussian filter ~ 280,000 km^2) is approximately 900 times greater than that of the average catchment in the study. Assuming a well measuring footprint of 150 meter radius, the associated spatial mismatch between well derived

measurements of storage and an average catchment area is roughly 4,500. Vadose zone storage dynamics are not captured in well data and are challenging to characterize with soil moisture probes due to the high degree of spatial variability. Due to the improved spatial resolution and ability to measure the entire hydrologic profile, it was hypothesized that the GRACE TWSA measurements are a valuable and novel measurement to estimate storage dynamics across the critical zone and subsurface aquifers in headwater catchments in the Sierra Nevada.

Geology data was used to interpret the hydrogeology of each catchment in the study area. Geologic data was acquired from the USGS California geological map (http://pubs.usgs.gov/of/2005/1305/#CA). The 52 lithologies that comprised the geologic map were re-classified into six categories: unconsolidated, extrusive, intrusive, sedimentary, metamorphic, and un-classified (Figure 19, Table 1). Unconsolidated, primarily alluvium, and extrusive geologies were interpreted as high storage capacity systems. Intrusive geologies, dominated by granites, were interpreted as low storage capacity systems. These three geologic categories, unconsolidated, extrusive, and intrusive compromised greater than 95 percent of all but one catchment. The hydrogeological interpretation of the low storage capacity systems is that the geologic media has low porosity and permeability but the formations has a potential for a high degree of fractured flow. In contrast, the high storage capacity catchments, dominated by volcanic and alluvial deposits, have geologic media that have high porosity and medium to high permeability with wide range in the potential for fracture flow. Assuming similar Mediterranean type precipitation regimes between the high and low storage capacity catchments, it is likely that, during the beginning of the recession period, the low storage capacity catchments have a greater hydraulic gradient than the high storage capacity catchments. This is a direct result of the higher porosity in the high storage capacity catchments. For a given amount of precipitation,

the low storage/low porosity catchment will “fill up” to a greater extent than the high storage/high porosity catchment. Therefore, the low storage capacity catchments will have a greater hydraulic gradient. Consequentially, the low storage capacity catchments may have similar or greater initial discharge rates relative to the high storage capacity catchments due to the increased hydraulic gradients, despite the differences permeability.

To remove the effect of surface water storage from the GRACE TWSA data, monthly volumetric reservoir data from the California Data Exchange Center database was compiled. The reservoir data was aggregated into a monthly volumetric reservoir anomaly time series for each 1 degree GRACE pixel. The volume anomaly associated with the reservoirs in each pixel was derived from the same time periods as the GRACE TWSA anomaly dataset (i.e. deviation from the 2004-2009 average). To apply these values to the TWSA dataset, they were processed with the same processing algorithm used to processes the GRACE dataset(see above: Swenson, 2011, 2002; Swenson et al., 2008). Therefore, a pixel specific scaling factor (Figure 20) was applied to each time series of total reservoir anomaly. The scaled reservoir anomaly time series were then applied to the TWSA dataset to produce a reservoir corrected TWSA time series (see Equation 8). Overall, the reservoir anomaly correction had a small impact on the TWSA time series.

Equation 8a: $TWSA(t) = TWSA_{res}(t) + TRSA(t)$

Equation 8b: $TRSA(t) = (S_f * [TRS_{ave} + TRS(t)]) / A_{pix}$

$TWSA(t)$ = Total Water Storage Anomaly without Reservoir Component
$TWSA_{res}(t)$ = Total Water Storage Anomaly with Reservoir Component
$TRSA(t)$ = Total Reservoir Storage Anomaly
TRS_{ave} = Total Reservoir Storage 2004-2009 average
$TRS(t)$ = Total Reservoir Storage
A_{pix} = GRACE 1 degree Pixel Area

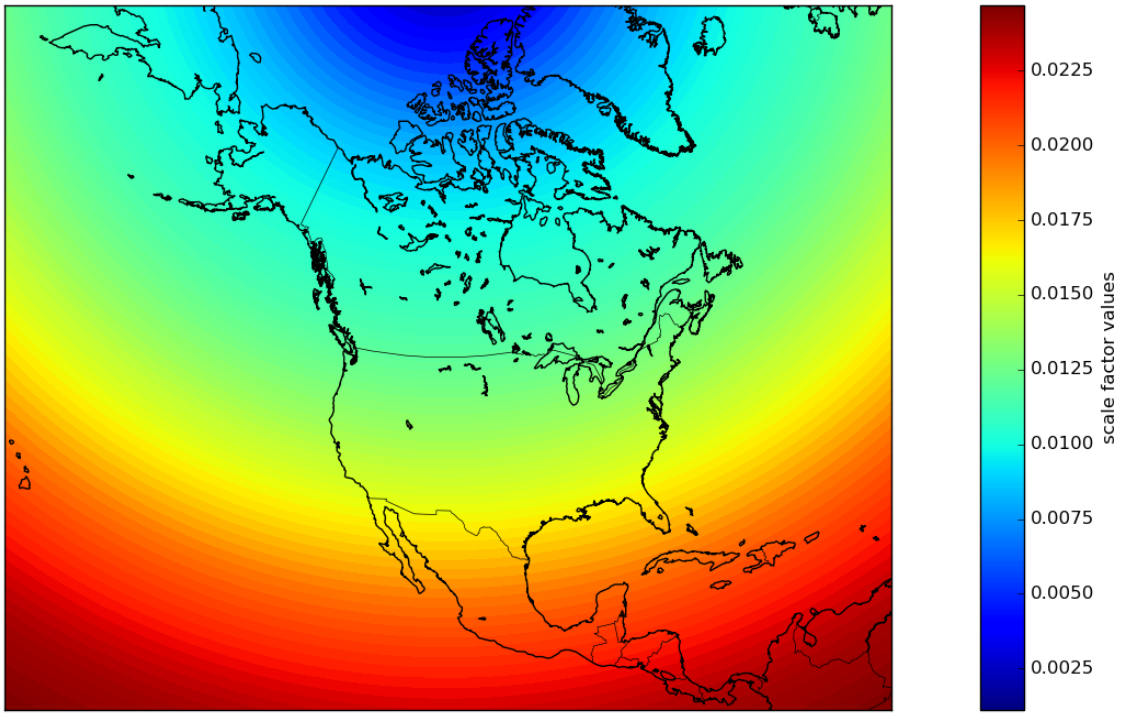

Figure 20: Scale factors used to calculate the reservoir anomaly correction to the TWSA.

Methods: Analysis

Low flows for each stream gage were calculated with the Y_7 flow statistic (see above). The storage anomaly time series at each catchment was computed from the TWSA dataset. If a catchment extended into more than one GRACE grid cell, an area average value of the TWSA data was computed. A linear interpolation of the TWSA data was used to downscale the temporal sampling frequency of the TWSA dataset to the date the Y_7 flow occurred at each catchment (see Figure 21 for an example). Congruent with the conceptual model that low flows are an expression of the storage regime, the Y_7 flow occurred at or very near to the annual minimum TWSA for nearly all years and catchments. The only consistent departure from this trend is the 2013 water. For many of the gages, the 2013 low flow occurred before the TWSA time series reached a minimum value.

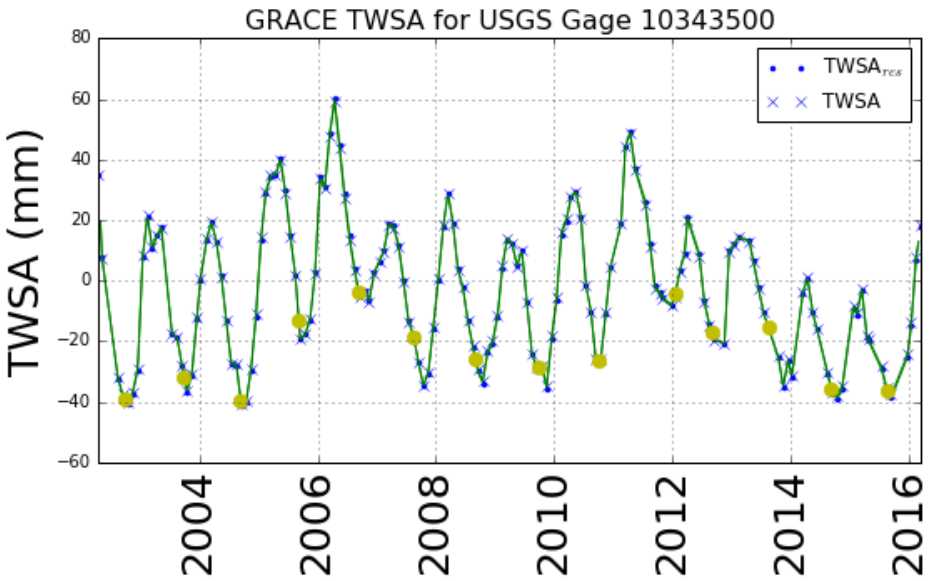

Figure 21: Example of the TWSA tie series for USGS gage 10343500. Dotted blue points represent the TWSA data and the blue crosses indicate the reservoir corrected TWSA time series. The green line is the interpolation of the TWSA dataset. The large yellow points indicate the timing of the Y_7 low flow for the 10343500 gage.

A power law function (Equation 9) was used to relate Y_7 flow to catchment TWSA. Equation 9 has physical basis from groundwater hydraulic theory and has been widely used throughout the scientific literature to relate flow and storage (Botter et al., 2009; Brutsaert, 2012, 2010, 2008; Brutsaert and Sugita, 2008). To convert the storage anomaly value of GRACE to a total storage metric, Equation 9 was modified to incorporate the storage anomaly term (Equation 10). Y_7 and TWSA were fit to Equation 10 with a Levenberg–Marquardt (non-linear least squares) technique. However, because there are three fitting variables (W_o, K, and N) the resulting solutions will likely be unconstrained. Therefore, the results of this procedure will be used to evaluate the correlation between the Y_7 flows and TWSA rather than capturing the absolute values of the W_o, K, and N parameters in Equation 10. As such, this procedure precludes the possibility of prescribing physical meaning to the W_o, K, and N parameters results.

Equation 9: $Y_7 = K * (S^N)$

Y_7 = 7 day average annual low flow
S = Subsurface Storage
N, K = Fitting parameter

Equation 10: $Y_7 = K* (TWSA - W_o)^N$

Y_7 = 7 day average annual low flow normalized to catchment area
Q = Volumetric stream flow
A = Catchment area
TWSA = Total Water Storage Anomaly
W_o = TWSA value at zero flow
N, K = Fitting parameter

To compare the storage-discharge results from space-based measurements of storage to that predicted by hydraulic groundwater theory using recession analyses (objective 3), the methodology pioneered by Brutseart and Neibar (1977) that relates a Boussinesq-Dupuit aquifer to stream flow recession was implemented. Stream flow recession is analyzed in a log -dY versus log Y space (Equation 11). Equation 11 is widely used to estimate stream flow recession and can easily be solved in log space with a best fit linear line. However, other studies have employed variations to this model to describe the recession (Kirchner, 2009).

Equation 11: $dY/dt = aY^b$

Y = Area normalized stream flow rate
a, b = fitting parameters

Limitations inherent to a Boussinesq-Dupuit aquifer make applying this recession approach to mountainous catchments problematic. The geometry and heterogeneity within the study catchments likely violate the assumptions associated with a Boussinesq-Dupuit solution. However, low flow conditions may be a unique case when applying a Boussinesq-Dupuit type aquifer are valid in mountainous catchments due to a reduced slope within the aquifer. For example, Mendoza et al. (2003) had success applying this methodology in mountainous catchments. Furthermore, theoretical work by Rupp and Selker (2006, 2005) has shown the

utility of applying this method to low-flow analysis in moderate to steep terrains and heterogeneous hydraulic properties. Both paper concluded, for long-time drainage, a numerical model of stream flow recession could be reduced to an analytical model, as in Equation 11.

To capture the recession dynamics at low flow conditions, the data was analyzed for the entire period of record at each stream gage that was less than 125 percent of the maximum Y_7 flow from the 2002 to 2015 period (in log space). To reduce the noise within the dataset, each measurement of recession was averaged at the discrete flow rates unique for each gage. Therefore, for each flow interval there is one corresponding measurement of the recession rate. The aggregated recession and flow rates where log transformed and a best fit line, in the form of Equation 11, was calculated for each gage. To estimate a realistic range for the intercept in Equation 11, a lower and upper envelope fit were calculated for each gage by varying the *a* parameter. The lower envelope line resulted in 95% of the observations above the line while the upper envelope line is greater than 5% of the observations.

The underlying mathematics behind the stream flow recession and Y_7 – TWSA relationships are both based on linear reservoir theory. Therefore, the consistency between the two analyses was evaluated and a more constrained the TWSA – Y_7 relationship was solved with physically realistic parameter values. Assuming evapotranspiration and rainfall are negligible fluxes during low flow conditions, the continuity equation (Equation 12) can be used to relate stream flow recession to storage dynamics. Following Clark et al. (2009), Equations 13 and 14 were used to relate the parameters in Equation 10 to Equation 11. Using 2 standard deviations from the slope (b parameter in Equation 11) and upper and lower intercept/envelope (a parameter in Equation 11) in the stream flow recession, the K and N parameters were constrained in the TWSA – Y_7 fitting routine. The Wo parameter was left as an unconstrained

parameter. By fitting the observed TWSA–Y_7 observations with the constrained parameter values from the recession analysis it will be tested if the two analyses are consistent as well as compute a unique solution to the TWSA–Y_7 relationship with physically meaningful parameters.

Equation 12: $dS/dt = -Q$

Results

On average across the study area, there were strong relationships between the TWSA and Y_7 flows (Figure 22). Of the 10 catchments in the study, 9 had moderate to good correlations between TWSA and Y_7 flow (r^2 greater than 0.4). Despite the relative mismatch in spatial and temporal scales, this study found compelling evidence that the spaced-based measurements of storage from the GRACE satellite are able to resolve the low flow dynamics in these relatively small Sierra Nevada catchments. Of the nine catchments with strong correlations, five were in low storage capacity catchments and four were in high storage capacity catchments. However, the best fit solutions to the TWSA – Y_7 relationship were highly unconstrained which resulted physically meaningless values for the N parameter (unrealistically large values) and the K parameter (unrealistically low values). The unconstrained nature of the results is due to the high degree of correlation between the fitting variables in Equation 10.

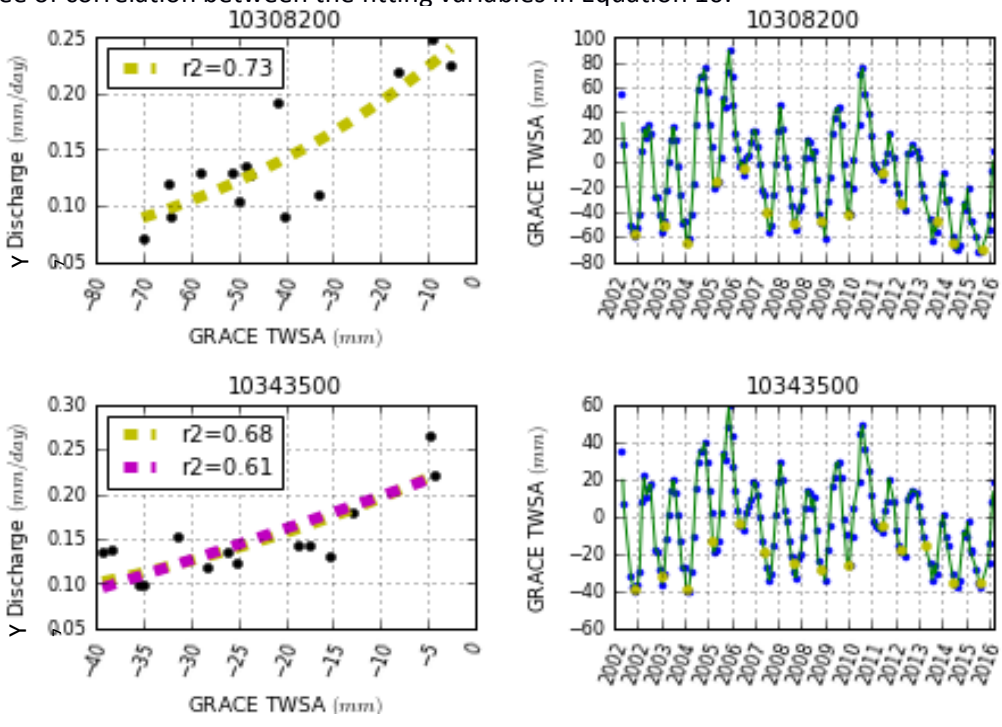

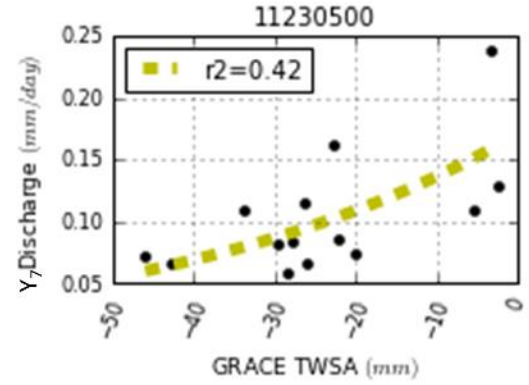
11230500
r2=0.42
Y7 Discharge (mm/day)
GRACE TWSA (mm)

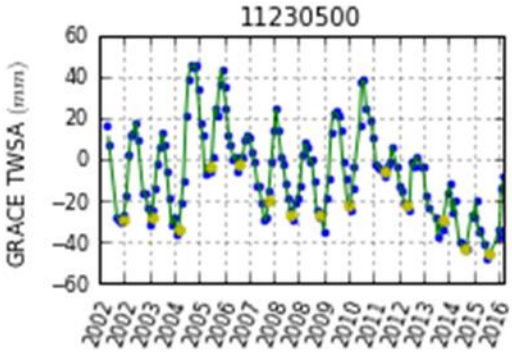
11230500
GRACE TWSA (mm)

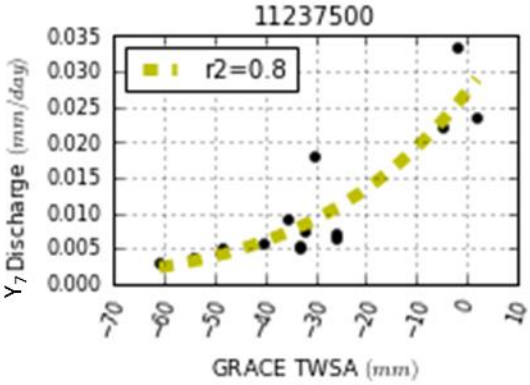
11237500
r2=0.8
Y7 Discharge (mm/day)
GRACE TWSA (mm)

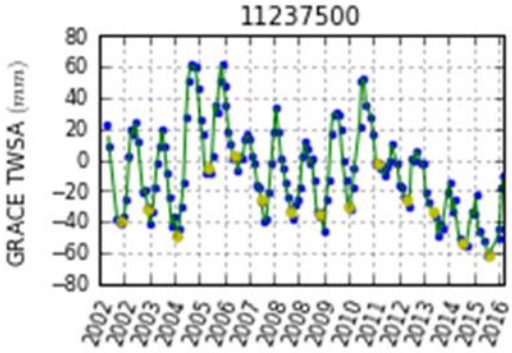
11237500
GRACE TWSA (mm)

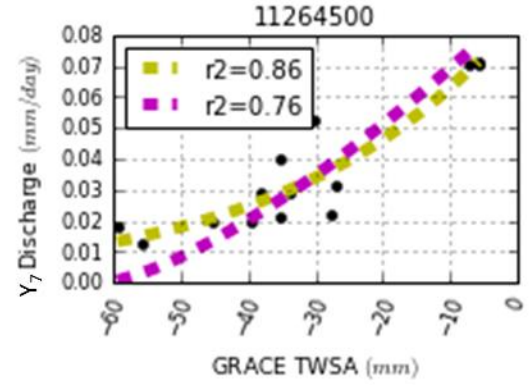
11264500
r2=0.86
r2=0.76
Y7 Discharge (mm/day)
GRACE TWSA (mm)

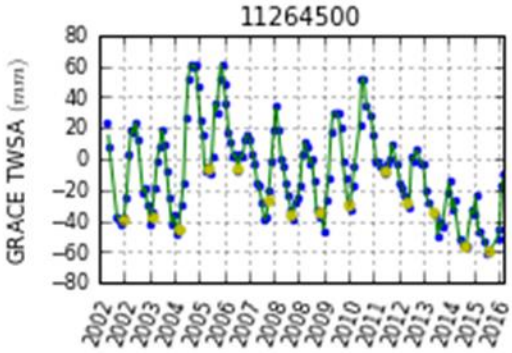
11264500
GRACE TWSA (mm)

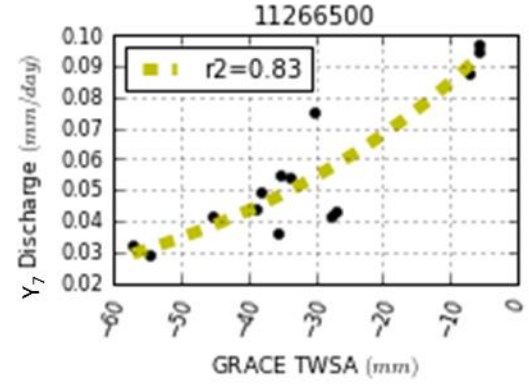
11266500
r2=0.83
Y7 Discharge (mm/day)
GRACE TWSA (mm)

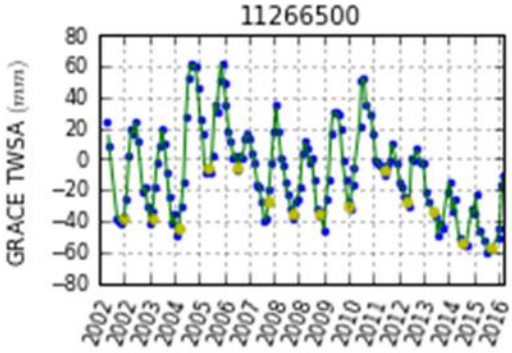
11266500
GRACE TWSA (mm)

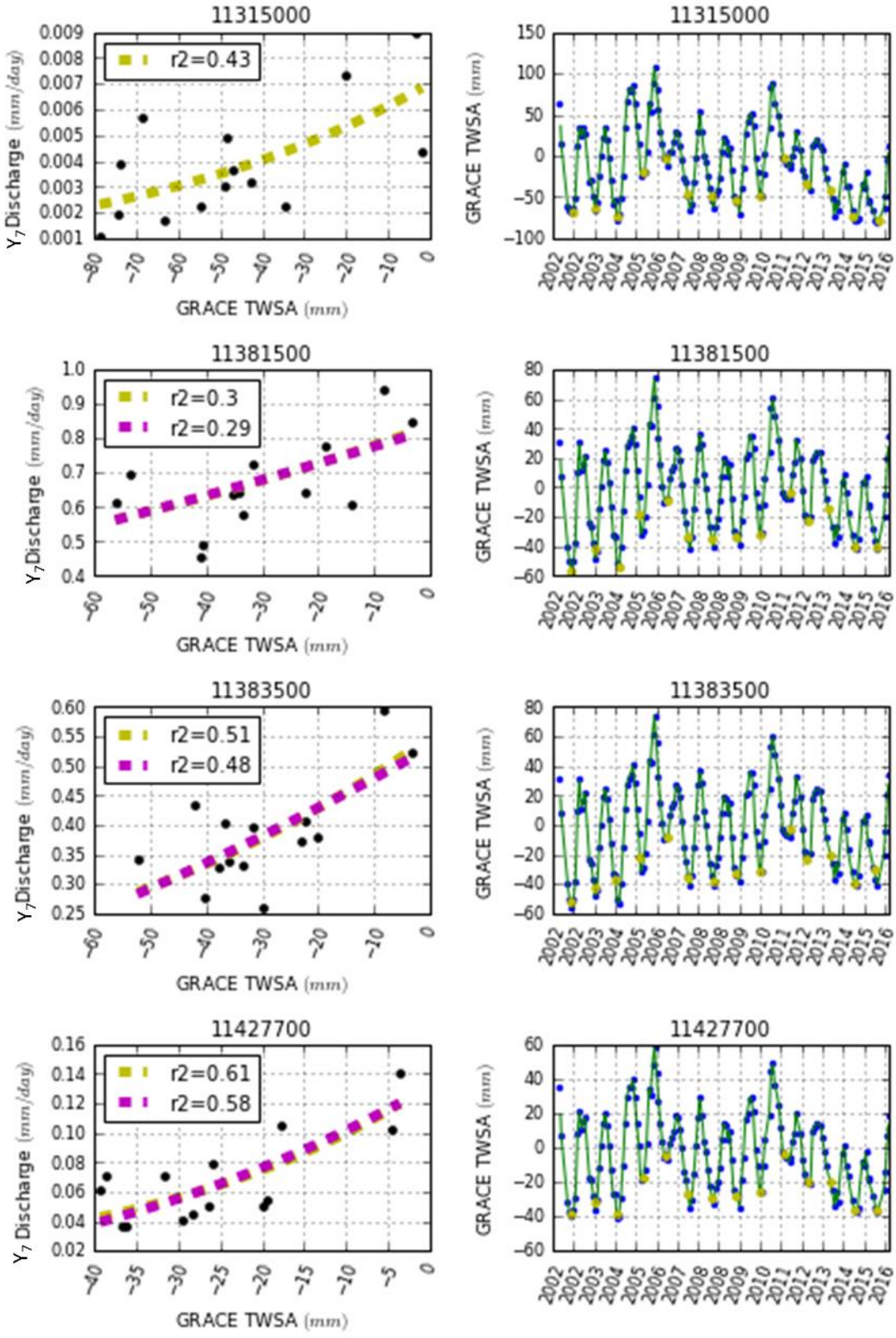
11315000
r2=0.43
Y7Discharge (mm/day)
GRACE TWSA (mm)
11315000
GRACE TWSA (mm)
11381500
r2=0.3
r2=0.29
Y7Discharge (mm/day)
GRACE TWSA (mm)
11381500
GRACE TWSA (mm)
11383500
r2=0.51
r2=0.48
Y7Discharge (mm/day)
GRACE TWSA (mm)
11383500
GRACE TWSA (mm)
11427700
r2=0.61
r2=0.58
Y7 Discharge (mm/day)
GRACE TWSA (mm)
11427700
GRACE TWSA (mm)

Figure 22: The results of the TWSA-Y_7 relationship are illustrated for each gage. Yellow lines indicate the best fit solution for the unconstrained model. Magenta lines indicate the best fit line for the constrained model. If the constrained model was unable to find a fit to the TWSA-Y_7 observations no line is shown. Figure 22 continues on next two pages. 1

Following Equation 11, a best fit line was calculated in log space for each gage as well as a upper and lower envelop model (Figure 23). The catchments in the study appear to exhibit a linear relationship in log space between recession and flow rates suggesting Equation 11 as a valid model. Using Equations 13 and 14, the range in recession parameters were converted to a corresponding range in TWSA – Y_7 parameters. Table 2 lists the results of the recession analysis and range in the a and b parameters for Equation 11, and K, and N for Equation 10.

Equation 13: $N = 1 / (2-b)$

Equation 14: $K = (a/N)^N$

Source	Gage	10308200	10343500	11230500	11237500	11264500	11266500	11315000	11381500	11383500	11427700
Recession Results	a min	2.40E-02	5.30E-02	7.72E-02	4.10E-02	6.58E-02	4.52E-02	7.62E-03	1.14E-02	1.45E-02	7.85E-02
	a best fit	9.06E-02	2.03E-01	2.37E-01	4.69E-01	4.93E-01	1.59E-01	7.29E-02	7.38E-02	1.11E-01	6.12E-01
	a max	3.47E-01	8.33E-01	1.17E+00	4.97E+00	4.57E+00	6.47E-01	7.45E-01	4.26E-01	5.89E-01	4.53E+00
	b min	8.81E-01	1.16E+00	1.16E+00	1.11E+00	1.29E+00	1.04E+00	5.14E-01	1.37E+00	1.38E+00	1.45E+00
	b best fit	9.68E-01	1.31E+00	1.25E+00	1.29E+00	1.43E+00	1.16E+00	7.32E-01	1.46E+00	1.48E+00	1.59E+00
	b max	1.06E+00	1.46E+00	1.33E+00	1.46E+00	1.57E+00	1.27E+00	9.50E-01	1.54E+00	1.57E+00	1.73E+00
	k min	1.81E-02	1.41E-03	1.15E-02	8.51E-04	2.82E-04	9.41E-03	1.00E-02	9.52E-06	6.87E-06	7.96E-07
	k best fit	3.45E-02	3.45E-02	3.45E-02	3.45E-02	3.45E-02	3.45E-02	3.45E-02	3.45E-02	3.45E-02	3.45E-02
	k max	4.29E-01	6.55E-01	9.80E-01	5.32E+00	5.24E+00	6.05E-01	1.07E+00	1.21E-01	1.93E-01	5.26E+00
	n min	1.83E+00	1.83E+00	1.83E+00	1.83E+00	1.83E+00	1.83E+00	1.83E+00	1.83E+00	1.83E+00	1.83E+00
	n best fit	9.69E-01	1.45E+00	1.33E+00	1.40E+00	1.74E+00	1.19E+00	7.89E-01	1.85E+00	1.92E+00	2.44E+00
	n max	3.66E+00	3.66E+00	3.66E+00	3.66E+00	3.66E+00	3.66E+00	3.66E+00	3.66E+00	3.66E+00	3.66E+00
Unconstrained Model Results	K	8.03E-58	1.60E-192	1.53E-80	7.58E-16	7.23E-101	1.00E-95	1.14E-42	1.58E-54	5.14E-112	1.02E-169
	N	1.83E+01	5.61E+01	2.58E+01	6.01E+00	3.27E+01	3.00E+01	1.33E+01	1.60E+01	3.25E+01	5.16E+01
	Wo	-1.23E+03	-2.55E+03	-1.16E+03	-1.80E+02	-1.07E+03	-1.36E+03	-9.80E+02	-2.30E+03	-2.62E+03	-1.80E+03
	R^2	7.33E-01	6.81E-01	4.24E-01	7.97E-01	8.60E-01	8.31E-01	4.29E-01	3.01E-01	5.07E-01	6.09E-01
Constrained Model Results	K	1.81E-02	1.41E-03	1.15E-02	8.51E-04	2.82E-04	9.41E-03	1.00E-02	9.52E-06	1.39E-04	7.96E-07
	N	9.69E-01	1.45E+00	1.33E+00	1.40E+00	1.74E+00	1.19E+00	7.89E-01	1.85E+00	1.92E+00	2.44E+00
	Wo	-7.01E+01	-7.39E+01	-4.60E+01	-6.09E+01	-6.11E+01	-5.71E+01	-7.86E+01	-3.16E+02	-1.62E+02	-1.05E+02
	R^2	-	6.06E-01	-	-	7.65E-01	-	-	2.92E-01	4.80E-01	5.84E-01

Table 2: Results from recession and TWSA – Y_7 analyses.

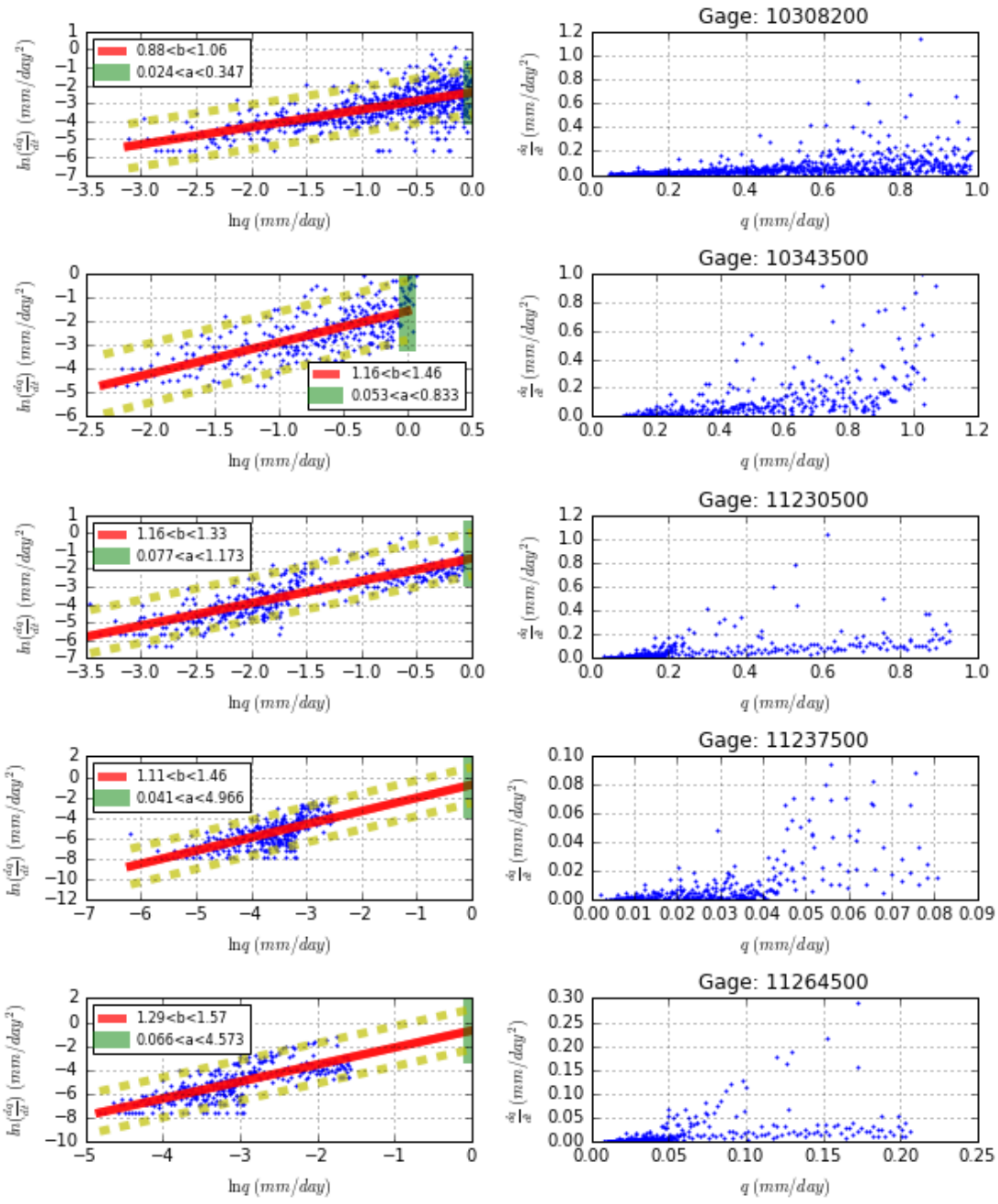

Figure 23: Recession analysis at each USGS gage in the study. For each gage the recession analysis in normal (column 1) and log space (column 2) are shown. The red line indicates the best fit model while the dotted yellow lines indicate the 5% and 95% envelope models. A two standard deviation range for each parameter in Equation 4 shown in each graph. Figure 23 continues on the next page

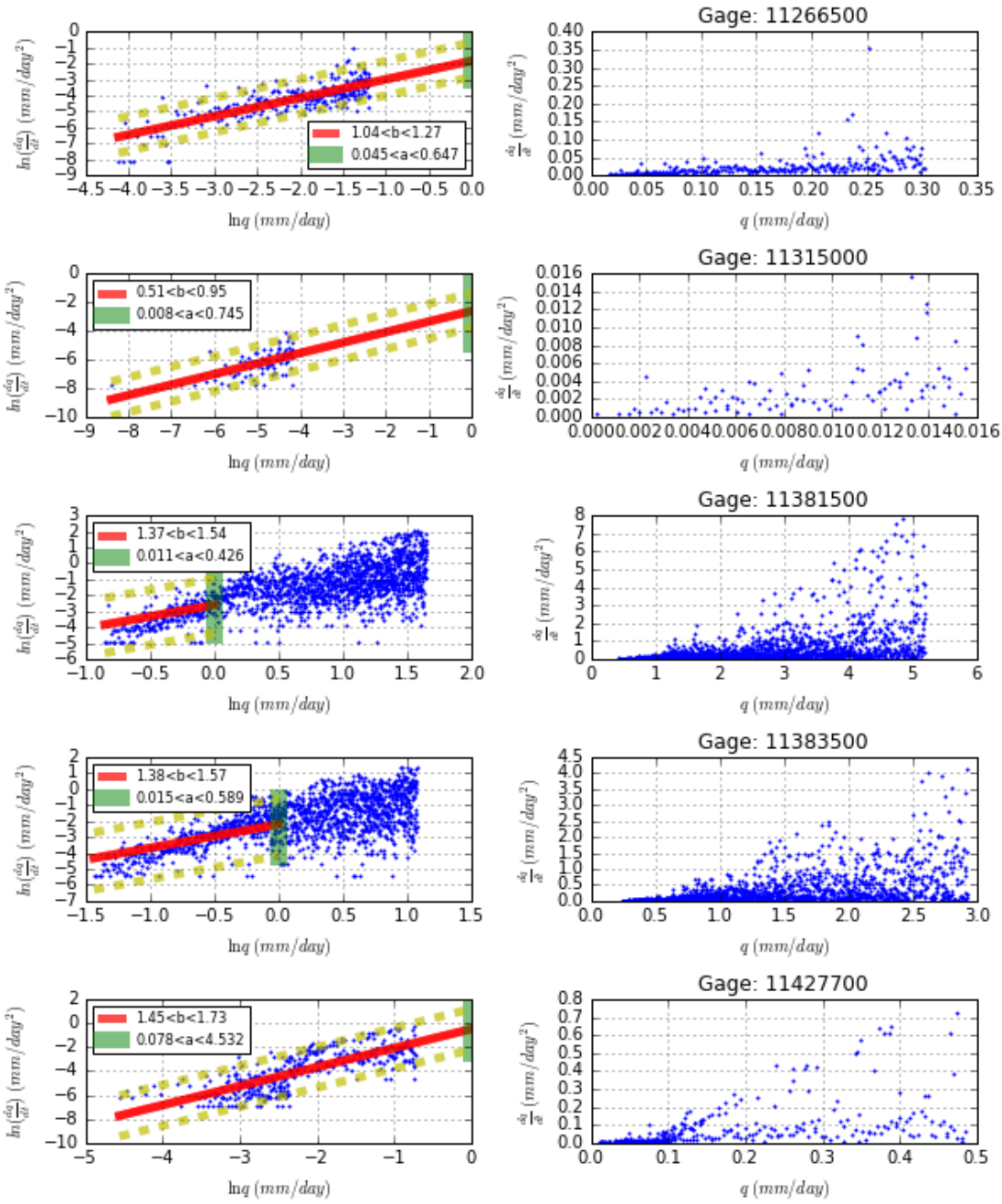

The parameter ranges defined in Figure 23 and Table 2 were then used to constrain the TWSA – Y_7 model. The minimum storage (Wo) parameter was left as an unconstrained variable while the N and K parameters where constrained. Implementing these constraints resulted in unique solutions to the TWSA – Y_7 relationships with r^2 values greater than 0.47 in 4 of the 10

catchments in the study. Therefore, in nearly half the catchments in the study, this study found that the recession dynamics, as predicted by hydraulic groundwater theory, were consistent with the observed relationships between space-based estimates of catchment storage and stream low flows. Of the four catchments with consistent results between the TWSA – Y_7 relationship and stream flow recession 3 were high storage capacity catchments and one was a low storage capacity catchment.

There was a strong discrepancy (difference) between the unconstrained and constrained models, due to differences in N and K parameters, when extending the TWSA - Y_7 relationship to the no flow boundary (Figure 24). The most notable difference between the unconstrained and constrained models is the degree of linearity resulting in substantial different zero flow storage values (Wo). The constrained models typical reach zero flow between -60 and -105 mm TWSA whereas the unconstrained models reach zero flows at much smaller values of TWSA (Table 2). The constrained models exhibit a much more linear relationship between storage and flow than the unconstrained models. The unconstrained models have very large N and very small K values. The extreme parameter values in the unconstrained models results in the inability to prescribe physical meaning to the N and K parameters. While the constrained model has a more physically meaningful basis, it does a poorer job matching the observations. Therefore, it is not clear which approach is more meaningful in estimating future low flow regimes. However, the no-flow threshold may not be a critical metric in low flow analysis. Rather, identifying threshold flows for ecological vitality, specific for each catchment, would likely be a more meaningful metric to identify the critical low-flow thresholds.

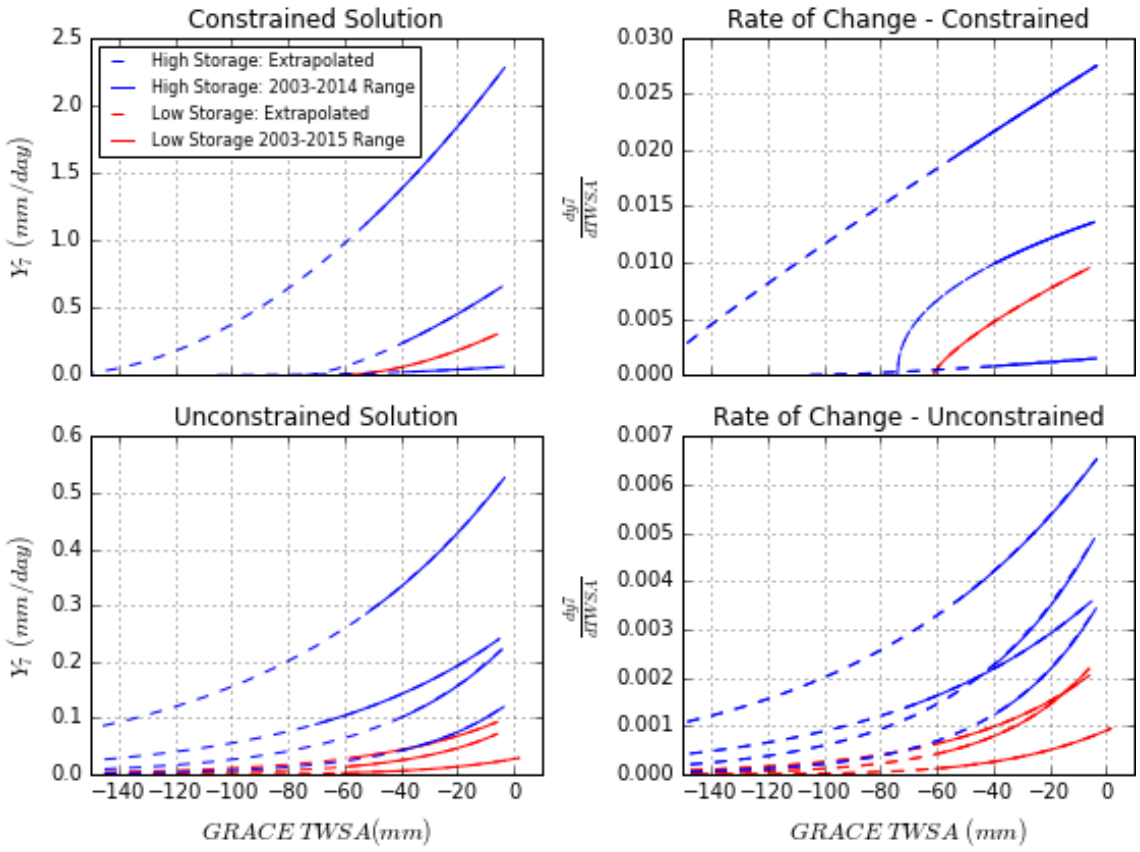

Figure 24: Shows the theoretical relationship between TWSA and flow (normalized by catchment area) for both the unconstrained and constrained models for catchments with r^2 values greater than .47. Solid lines indicate the historical (2003-2015) storage range during low flows. The dashed lines extend the relationship to twice the historical range in storage and indicate potential flows at increasing levels of drought severity.

In addition to the total magnitude, the net reduction in flow is a critical component in considering the impacts of climate change on low flow regimes. Figure 24 indicates that, in general, the high storage capacity catchments experience the greatest rate of stream flow reduction with increasing drought severity. This is most visible in the rate of stream flow reduction as a function of TWSA ($dY_7/dTWS$). Of the three high storage capacity catchments, two experience stream flow reduction at rates 2 to 3 times greater than that of the low storage capacity catchments. This result is consistent with assumption that high storage capacity

catchments can hold greater volumes of water and are able to convert storage to stream flow at a much higher rate. High storage capacity catchments are thus able to maintain high rates of drainage during long drought periods. Therefore, when transitioning from historical low flow regimes to the current and more extreme drought conditions expected in the future, it may be the high storage capacity catchments that experience a greater net effect on stream flow reduction than the low storage capacity catchments.

Discussion

Despite the spatial and temporal mismatch between the storage observations derived from the GRACE satellite and low flow dynamics of unimpaired streams in the Sierra Nevada, there are compelling correlations that suggest the TWSA measurements are able to resolve annual low flows. The Sierra Nevada Range provided an ideal study area due to the Mediterranean climate that results in relatively consistent late summer conditions. This allowed attribution of the GRACE signal during low flows to subsurface storage dynamics. Furthermore, recession analysis derived from hydraulic groundwater theory provided an opportunity to constrain the parameterization of the TWSA – Y_7 model as well as show a consistency between two independent approaches to relate flow dynamics to catchment storage. While both analyses contain methodological weaknesses, comparing the results of these two disparate approaches increased the confidence in the results.

Storage – flow dynamics are likely to have a strong influence on future flow regimes across the Sierra Nevada. Due to a changing climate, predicted snow-pack reduction and increased temperatures across the Sierra Nevada (Leung et al., 2004) will likely result in more frequent and uncharacteristically severe hydrologic droughts in the future. Therefore, the current historic drought (2012 – current) may provide insight to future low flow regimes. As

evident in Figure 24, the high storage capacity catchments appear to be at a greater risk for reduced flows at increasing levels severe drought. Conversely, because the low storage capacity catchments have historically already reached very low flow conditions, they are likely to see a smaller magnitude in their reduction of flow with increasing drought severity (Tague and Grant, 2009). Interpreting the susceptibility a low versus high storage capacity catchments to ecological degradation is not clear. While the low storage capacity catchments likely have smaller flow rates, the ecology may be well adapted for low flow conditions. Whereas, the high storage capacity communities may not be well adapted for the predicted decreases in flow rates.

Interpretations and application of these results should be carefully considered in the context of the uncertainty inherent to this study. The spatial mismatch between the study catchments and the GRACE footprint may contribute a substantial degree of error to the analysis. The spatial extents of the GRACE footprint for an individual pixel likely extend outside the Sierra Nevada Mountains into the San Joaquin Valley to the West and/or the Great Basin to the East. Due to the differential climates and geologies across these regional-scale basins, the storage dynamics in the San Joaquin Valley and Great Basin may be substantially different than that of the catchments in the study. As previously discussed, the same degree of spatial mismatch is also present when using well measurements to characterize storage. However, a well or network of wells, may be more desirable to characterize storage due to the likely spatially correlation to the storage dynamics across the catchment. Therefore, while the magnitude of the storage dynamics as measured from a well may not be accurate, the phase and trends will likely be a good representation of catchment storage. Conversely, the spatial correlation between the Sierra Nevada catchments and the San Joaquin Valley/Great Basin is unknown. However, because the effect of mass on gravity is attenuated at a rate of one divided

by the radius squared, it is a reasonable assumption that the storage dynamics in the San Joaquin Valley and Great Basin are substantially attenuated within the mass anomaly measurements across the Sierra Nevada. Therefore, while attributing the GRACE measurements across the Sierra Nevada directly to small catchments within the Sierra Nevada does contain a degree of error, it provides a significant and novel measurement of storage dynamics that are notoriously difficult to characterize (McNamara et al., 2011). Considering the lack of well networks within the Sierra Nevada and the HCDN catchments, the GRACE measurements are currently the only observations of storage that can be incorporate into hydrologic analyses in this and many other regions.

There are problematic assumptions in applying the results of the stream flow recession analysis to the storage – flow model. As previously discussed, the Boussinesq-Dupoit assumptions are likely violated within small mountainous catchments. However, as previously cited (Rupp and Selker, 2006, 2005), numerical analysis has suggested that the linear reservoir model and stream flow recession may be a valid approach for sloping aquifers with heterogeneous hydraulic conductivity. Within this framework, the N term in Equation 10 is related to the exponential decay in hydraulic conductivity with depth. However, the geologic complexity that likely exists within these catchments would suggest that a simple continuous analytical model of hydraulic conductivity as a function of depth may not be sufficient. , Extrapolating these results beyond the observed flow conditions may thus be problematic. Furthermore, applying the continuity equation (Equation 12) to relate stream flow recession to the linear reservoir model of storage and flow assumes the only flux of water out of a catchment is stream flow, yet evapotranspiration, even during the late summer, is likely a substantial

component in the water balance. Therefore, better methods are needed to characterize evapotranspiration and relate it to the linear reservoir theory of storage and stream flow.

Considering these limitations, it remains a novel finding that the GRACE measurements of TWSA are highly correlated to stream low flows and are generally consistent with predictions derived from hydraulic groundwater theory. This research provides a first step in developing more robust methods to quantifying storage dynamics. Storage dynamics are largely overlooked in many watershed water-balance type analyses. For instance, Condon and Maxwell, (2016) found that storage and groundwater flow was an important component in developing Budyko curves. Water budget analyses that did not directly account for groundwater dynamics produced budyko type behavior however the curve parameters where substantially impacted when groundwater flows where incorporated. Furthermore, regional patterns resulting from Budyko analyses where also altered when groundwater-surface water interactions where directly incorporated into the analyses. In addition, many distributed hydrologic models implement a “bucket” approach to allocate storage to baseflow. To fit these models to flow observations, the storage to baseflow process is commonly reduced to calibration parameters. Constraining the storage – flow dynamics to physically based measurements may improve the degree of parsimony and improve model performance/predictions. Quantifying the storage – flow relationship is critical to improving hydrologic analyses and predictions, specifically in estimating Sierra Nevada flow regimes in a warmer climate with significantly reduced snow packs.

The results of both chapters of this thesis (forest structure on soil moisture storage/recession as well as the storage-flow analysis of headwater catchments) indicate the critical importance of better quantifying the impact of a changing climate on water and

ecological resources. Both studies illustrate how the rate of change (soil moisture and stream flow recession) and timing (initiation of recession) are critical to the overall health of these systems (forests and headwater catchments). Climate change is fundamentally altering the forcing parameters (net energy and mass flux) within the hydrologic system. Therefore, it is critical to better quantify and classify how the internal dynamics of these systems will respond to the unprecedented environmental change. Only then can managers and communities develop strategies to mitigate the negative outcomes to the ecological and water resources as a direct result of a rapidly changing climate.

References

Allen, C.D., Macalady, A.K., Chenchouni, H., Bachelet, D., McDowell, N., Vennetier, M., Kitzberger, T., Rigling, A., Breshears, D.D., Hogg, E.H. (Ted), Gonzalez, P., Fensham, R., Zhang, Z., Castro, J., Demidova, N., Lim, J.-H., Allard, G., Running, S.W., Semerci, A., Cobb, N., 2010. A global overview of drought and heat-induced tree mortality reveals emerging climate change risks for forests. For. Ecol. Manag. 259, 660–684. doi:10.1016/j.foreco.2009.09.001

Bales, R., Goulden, M., Hunsaker, C.T., Conklin, M.H., Hartsough, P.C., O'Geen, A.T., Hopmans, J.W., Safeeq, M., 2015. Drought effects on evapotransiration and subsurface water storage in the southern Sierra Nevada (2015 AGU Fall Meeting).

Botter, G., Porporato, A., Rodriguez-Iturbe, I., Rinaldo, A., 2009. Nonlinear storage-discharge relations and catchment streamflow regimes: STREAMFLOW REGIMES OF NONLINEAR CATCHMENT. Water Resour. Res. 45, n/a–n/a. doi:10.1029/2008WR007658

Brutsaert, W., 2012. Are the North American deserts expanding? Some climate signals from groundwater storage conditions: ARE THE NORTH AMERICAN DESERTS EXPANDING? Ecohydrology 5, 541–549. doi:10.1002/eco.263

Brutsaert, W., 2010. Annual drought flow and groundwater storage trends in the eastern half of the United States during the past two-third century. Theor. Appl. Climatol. 100, 93–103. doi:10.1007/s00704-009-0180-3

Brutsaert, W., 2008. Long-term groundwater storage trends estimated from streamflow records: Climatic perspective: LONG-TERM GROUNDWATER STORAGE TRENDS. Water Resour. Res. 44, n/a–n/a. doi:10.1029/2007WR006518

Brutsaert, W., Nieber, J., 1977. Regionalized Drought Flow Hydrographs From a Mature Glaciated Plateau [WWW Document]. URL http://onlinelibrary.wiley.com/store/10.1029/WR013i003p00637/asset/wrcr2176.pdf?v=1&t=i9hg6b81&s=683c848e7334d8f7160a47a840da3da173e87518 (accessed 5.9.15).

Brutsaert, W., Sugita, M., 2008. Is Mongolia's groundwater increasing or decreasing? The case of the Kherlen River basin / Les eaux souterraines de Mongolie s'accroissent ou

décroissent-elles? Cas du bassin versant la Rivière Kherlen. Hydrol. Sci. J. 53, 1221–1229. doi:10.1623/hysj.53.6.1221

Cayan, D.R., Maurer, E.P., Dettinger, M.D., Tyree, M., Hayhoe, K., 2008. Climate change scenarios for the California region. Clim. Change 87, 21–42. doi:10.1007/s10584-007-9377-6

Clark, M.P., Rupp, D.E., Woods, R.A., Tromp-van Meerveld, H.J., Peters, N.E., Freer, J.E., 2009. Consistency between hydrological models and field observations: linking processes at the hillslope scale to hydrological responses at the watershed scale. Hydrol. Process. 23, 311–319. doi:10.1002/hyp.7154

Condon, L.E., Maxwell, R.M., 2016. Analyzing the impact of groundwater flow and storage changes on Budyko relationships across the continental US. Hydrol. Earth Syst. Sci. Discuss. 1–40. doi:10.5194/hess-2016-408

Decagon Devices, Inc., 2016. EC-5 Soil Moisture Sensor, Operator's Manual.

Dettinger, M.D., Cayan, D.R., Meyer, M.K., Jeton, A.E., 2004. Simulated hydrologic responses to climate variations and change in the Merced, Carson, and American River basins, Sierra Nevada, California, 1900–2099. Clim. Change 62, 283–317.

Garcia, E.S., Tague, C.L., 2015. Subsurface storage capacity influences climate–evapotranspiration interactions in three western United States catchments. Hydrol. Earth Syst. Sci. 19, 4845–4858. doi:10.5194/hess-19-4845-2015

Grant, G.E., Jones, J.A., 1996. Peak flow responses to clear-cutting and roads in small and large basins, western Cascades, Oregon. Water Resour. Res. 32, 959–974.

Green, S., 1998. HortResearch Institute Private Bag 11-030 Palmerston North New Zealand.

Kathleen S. Morse, 2008. North 49 Forest Health Recovery Project - Record of Decision and Environmental Impact Statement. United States Forest Service.

Kirchner, J.W., 2009. Catchments as simple dynamical systems: Catchment characterization, rainfall-runoff modeling, and doing hydrology backward: CATCHMENTS AS SIMPLE DYNAMICAL SYSTEMS. Water Resour. Res. 45, n/a–n/a. doi:10.1029/2008WR006912

Leung, L.R., Qian, Y., Bian, X., Washington, W.M., Han, J., Roads, J.O., 2004. Mid-century ensemble regional climate change scenarios for the western United States. Clim. Change 62, 75–113.

Lundquist, J.D., Dickerson-Lange, S.E., Lutz, J.A., Cristea, N.C., 2013. Lower forest density enhances snow retention in regions with warmer winters: A global framework developed from plot-scale observations and modeling. Water Resour. Res. 49, 6356–6370. doi:10.1002/wrcr.20504

McDowell, N., Pockman, W.T., Allen, C.D., Breshears, D.D., Cobb, N., Kolb, T., Plaut, J., Sperry, J., West, A., Williams, D.G., Yepez, E.A., 2008. Mechanisms of plant survival and mortality during drought: why do some plants survive while others succumb to drought? New Phytol. 178, 719–739. doi:10.1111/j.1469-8137.2008.02436.x

McNamara, J.P., Tetzlaff, D., Bishop, K., Soulsby, C., Seyfried, M., Peters, N.E., Aulenbach, B.T., Hooper, R., 2011. Storage as a Metric of Catchment Comparison. Hydrol. Process. 25, 3364–3371. doi:10.1002/hyp.8113

Memsic Inc., n.d. eKo Weather Station Suite.

Mendoza, G.F., Steenhuis, T.S., Walter, M.T., Parlange, J.-Y., 2003. Estimating basin-wide hydraulic parameters of a semi-arid mountainous watershed by recession-flow analysis. J. Hydrol. 279, 57–69. doi:10.1016/S0022-1694(03)00174-4

Monteith, J.L., 1965. Evaporation and environment. Symp. Soc. Exp. Biol. 19, 205–224.

NFP (National Fire Plan) [WWW Document], 2010. URL https://www.forestsandrangelands.gov/resources/overview/ (accessed 1.29.16).

Pal, I., Towler, E., Linveh, B., 2015. How Can We Better Understand Low River Flows as Climate Changes? - Eos. Earth Space Sci. News 96. doi:10.1029/2015EO033875

Park Williams, A., Allen, C.D., Macalady, A.K., Griffin, D., Woodhouse, C.A., Meko, D.M., Swetnam, T.W., Rauscher, S.A., Seager, R., Grissino-Mayer, H.D., Dean, J.S., Cook, E.R., Gangodagamage, C., Cai, M., McDowell, N.G., 2012. Temperature as a potent driver of regional forest drought stress and tree mortality. Nat. Clim. Change 3, 292–297. doi:10.1038/nclimate1693

P. C. D. Milly, Betancourt, J., Falkenmark, M., Hirsch, R.M., Kundzewicz, Z.W., Lettenmaier, D.P., Stouffer, R.J., 2008. Stationarity Is Dead: Whither Water Management? Science 319, 573–574. doi:10.1126/science.1151915

Rupp, D.E., Selker, J.S., 2006. On the use of the Boussinesq equation for interpreting recession hydrographs from sloping aquifers: BOUSSINESQ EQUATION FOR SLOPING AQUIFERS. Water Resour. Res. 42, n/a–n/a. doi:10.1029/2006WR005080

Rupp, D.E., Selker, J.S., 2005. Drainage of a horizontal Boussinesq aquifer with a power law hydraulic conductivity profile: DRAINAGE OF A HORIZONTAL BOUSSINESQ AQUIFER. Water Resour. Res. 41, n/a–n/a. doi:10.1029/2005WR004241

Slack, J.R., Landwehr, J.M., 1992. Hydro-Climatic Data Network (HCDN): A U.S. Geological Survey Streamflow Data Set for the United States for the Study of Climate Variations, 1874-1988, Tech. rep., USGS [WWW Document]. URL http://pubs.usgs.gov/of/1992/0129/report.pdf (accessed 5.11.15).

Smakhtin, V.U., 2001. Low flow hydrology: a review. J. Hydrol. 240, 147–186.

Steve Green, Brent Clothier, Bryan Jardine, 2003. Theory and Practical Application of Heat Pulse to Measure Sap Flow. Agron. J. 95, 1371.

Swenson, S., 2011. Restoring signal loss in grace terrestrial water storage estimates. Hydrol. Earth Syst. Sci. Discuss. 8, 2011.

Swenson, S., 2002. Methods for inferring regional surface-mass anomalies from Gravity Recovery and Climate Experiment (GRACE) measurements of time-variable gravity. J. Geophys. Res. 107. doi:10.1029/2001JB000576

Swenson, S., Chambers, D., Wahr, J., 2008. Estimating geocenter variations from a combination of GRACE and ocean model output. J. Geophys. Res. 113. doi:10.1029/2007JB005338

Tague, C., Grant, G.E., 2009. Groundwater dynamics mediate low-flow response to global warming in snow-dominated alpine regions. Water Resour. Res. 45. doi:10.1029/2008WR007179

Tague, C., Grant, G., Farrell, M., Choate, J., Jefferson, A., 2008. Deep groundwater mediates streamflow response to climate warming in the Oregon Cascades. Clim. Change 86, 189–210. doi:10.1007/s10584-007-9294-8

Vereecken, H., Huisman, J.A., Bogena, H., Vanderborght, J., Vrugt, J.A., Hopmans, J.W., 2008. On the value of soil moisture measurements in vadose zone hydrology: A review: SOIL MOISTURE AND HYDROLOGY. Water Resour. Res. 44, n/a–n/a. doi:10.1029/2008WR006829

Westerling, A.L., Hidalgo, H.G., Cayan, D.R., Swetnam, T.W., 2006. Warming and Earlier Spring Increase Western U.S. Forest Wildfire Activity. Science 313, 936–940. doi:10.1126/science.1130691